Adaptive behavior in turning of an oscillator-driven biped robot

Shinya Aoi · Kazuo Tsuchiya

Abstract This paper concentrates on a biped robot's turning behavior that consists of straight and curved walking and the transition between these two patterns. We investigate how a robot achieves adaptive walking during such turning by focusing on rhythm control and propose a locomotion control system that generates robot motions by rhythmic signals from internal oscillators and modulates signal generation based on touch sensor signals. First, we verify that the robot attains limit cycles of straight and curved walking by numerical simulations and hardware experiments. Second, we examine the transition between these walking patterns based on the basin of attraction of the limit cycles in numerical simulations. Finally, we verify whether the robot actually accomplishes transition and turning by hardware experiments. This paper clarifies that the robot establishes such turning motions by adequate modulation of walking rhythm and phase through interactions between the dynamics of its mechanical system, oscillators, and environment.

Keywords Biped robot · Adaptive behavior · Nonlinear oscillators · Phase reset · Turning · Curved walking · Limit cycle · Basin of attraction

S. Aoi (✉) · K. Tsuchiya
Department of Aeronautics and Astronautics, Graduate School of
Engineering, Kyoto University, Yoshida-honmachi, Sakyo-ku,
Kyoto 606-8501, Japan
e-mail: shinya_aoi@kuaero.kyoto-u.ac.jp

K. Tsuchiya
e-mail: tsuchiya@kuaero.kyoto-u.ac.jp

1 Introduction

Recently, the popularity of studies on biped robots have increased due to such challenges as inherent poor stability, the cooperation of a large number of DOF, nonlinearity in dynamics, and intermittent constraints of foot contact. Furthermore, recent advances in hardware and software technology allow these problems to be tackled, accelerating the interest. Actually, many sophisticated biped robots have already been developed that have successfully achieved various motions.

1.1 Turning behavior

In this paper, we focus on the turning behavior of a biped robot while it changes walking direction, which is one of the most fundamental robot behaviors. In particular, we deal with dynamic turning where a robot changes walking direction while moving forward. Such turning is accomplished when the robot's walking changes from straight walking to another direction, which is established by temporarily changing its walking from straight to curved and then varying it in another straight walking direction (Imai et al. 2001), as shown in Fig. 1. That is, this motion consists of straight and curved walking and the transition between these two patterns.

Stable periodic motions such as walking generate stable limit cycles in state space. Therefore, locomotion control of a biped robot implies limit cycle control (Brockett 2003; Laszlo 1996). Since different periodic motions such as straight and curved walking have different limit cycles, the transition between different periodic motions is the same as the transition between different limit cycles. Even if a robot establishes periodic motions and stable limit cycles, their transition is not necessarily confirmed. Therefore, the key
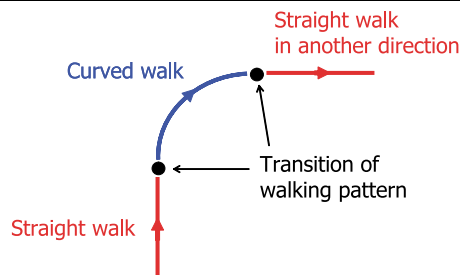
Fig. 1 Schematic of turning: during turning, robot changes walking direction by altering walking pattern between straight and curved. It is comprised of straight and curved walking and the transition between them

issue to achieve turning motion is confirming the transition between straight and curved walking.

So far, many studies have developed locomotion controllers, which establish not only straight walking but also turning, that were verified using hardware experiments (Hirai et al. 1998; Ishida et al. 2003; Kagami et al. 2002; Kajita et al. 2002; Löffler et al. 2003; Seara and Schmidt 2004). Most are based on model-based approaches that use inverse kinematics and kinetics and basically generate robot motions based on such criteria as zero moment point (Vukobratović et al. 1990). However, they require accurate modeling of both the robot and the environment as well as complicated computations, and the difficulty of achieving adaptability to various real world environments is often pointed out.

1.2 Adaptive behavior due to rhythm control

In contrast to robots, animals adapt themselves to various environments by cooperatively manipulating their complicated and redundant musculoskeletal systems. In neurophysiology, many studies have elucidated the control mechanism of animal walking, revealing that it is generated by central pattern generators (CPGs) (Grillner 1981, 1985, Orlovsky et al. 1999). CPGs are comprised of a set of neural oscillators present in the spinal cord and characteristically have the following properties:

1. CPGs are responsible for neural activity to generate rhythmic motor patterns that activate their limbs;
2. Sensory feedback from peripheral nerves modulates the neural activity of the CPGs.

Animals can immediately adapt to environmental changes and disturbances by virtue of these features and establish robust walking.

CPGs have been widely modeled using nonlinear oscillators. Taga et al. analyzed human walking using many links connected to each other through rotational joints and a network of nonlinear oscillators (Taga et al. 1991, 1995a, 1995b). Their numerical simulations showed that bipedal

walking is obtained by mutual entrainment between the dynamics of the musculoskeletal system, the oscillator network, and the environment. Ogihara and Yamazaki realized bipedal walking using a more physiological and anatomical model (Ogihara and Yamazaki 2001). Yamasaki et al. simulated bipedal walking using the CPG model and investigated the functional roles of CPG's phase reset to achieve robust walking (Yamasaki et al. 2003). Tomita and Yano carried out numerical simulations by incorporating a basal ganglia model (Tomita and Yano 2004).

As well as for human bipedal walking, CPG models have also been used to design control systems for walking robots. Fukuoka et al. and Kimura et al. developed quadruped robots and achieved adaptive quadrupedal walking on irregular terrain by employing CPG and reflex models (Fukuoka et al. 2003; Kimura et al. 1999). Lewis and Bekey created a quadruped robot that accomplished adaptive walking by a distributed control system composed of a CPG network using nonlinear oscillators (Lewis and Bekey 2002). Tsujita et al. proposed a locomotion control system for a quadruped robot using nonlinear oscillators and built a quadruped robot that obtained adaptive walking by changing the gait pattern to reflect walking speed and environmental variations (Tsujita et al. 2001). Akimoto et al. constructed a locomotion controller for a hexapod robot and realized an adaptive gait pattern based on walking speed (Akimoto et al. 1999). Inagaki et al. developed a decentralized six-legged robot and generated a gait pattern for it through their CPG model (Inagaki et al. 2003). Crespi et al., Ijspeert et al., and Inoue et al. created salamander and snake-like robots that accomplished serpentine meandering locomotion through a neural oscillator network (Crespi et al. 2005; Ijspeert et al. 2005, 2007; Inoue et al. 2004).

CPG models are also used to control biped robots. Lewis et al. built a biped robot that achieved two-dimensional bipedal walking generated by a silicon CPG chip and sensory signals (Lewis et al. 2003). Nakanishi et al. developed a biped robot that also obtained two-dimensional bipedal walking by employing nonlinear oscillators and phase reset (Nakanishi et al. 2004). Righetti and Ijspeert proposed a locomotion control system for a biped robot using nonlinear oscillators based on a learning framework (Righetti and Ijspeert 2006).

As cited above, many studies have developed bipedal locomotion controllers and analyzed locomotion based on CPG models by numerical simulations and hardware experiments. Although they accomplished significant walking adaptability, their control systems tend to be complicated with intricate essentials. On the contrary, we proposed a simple control system for a biped robot by referring to the above CPG characteristics and established adaptive straight walking against environmental variations and disturbances (Aoi and Tsuchiya 2005). Furthermore, not only based on

hardware experiments, we also clarified such dynamical characteristics based on analytical approaches using simplified models (Aoi and Tsuchiya 2006a, 2006b, 2007).

1.3 Adaptive behavior due to muscle tone control

From neurophysiology, it has been revealed that as well as rhythm control, muscle tone control also plays an important role in generating adaptive motions (Mori 1987; Rossignol 1996; Takakusaki et al. 2003, 2004), suggesting the importance of compliance in walking. Actually, many studies on robotics have demonstrated the essential roles of compliance. Specifically, by appropriately employing the mechanical compliance of robots, simple control systems attained highly adaptive, robust, and agile motions, especially in multi-legged (Aoi et al. 2007), hexapod (Altendorfer et al. 2001; Cham et al. 2004; Quinn et al. 2003; Saranli et al. 2001), quadruped (Fukuoka et al. 2003; Kimura et al. 1999; Poulakakis et al. 2005), and biped robots (Takuma and Hosoda 2006; Wisse et al. 2005).

As mentioned above, many researchers have been inspired by biologically and physiologically obtained results and actually achieved adaptive robot walking. However, note that most of these robots are controlled by motors whose actuators are completely different from animal muscles. In motor control, robot joints are generally manipulated so that they follow the desired trajectories by incorporating local high-gain feedback control. Since this means that robot motions are kinematically determined, it is difficult for motors to adequately control compliance during walking. However, robots easily modify their walking rhythm by modulating kinematical trajectories based on sensory information. Therefore, for motor-driven robots, developing a control system by focusing on walking rhythm based on biological and physiological results may be one method to establish adaptive walking.

1.4 This study's approach

Adaptive behavior requires adequate modulations of motion and response depending on such situations as walking speed and direction, physical properties, and the environmental situation. As mentioned above, general model-based approaches have difficulty achieving adaptability, meaning that in these approaches the robot is too *rigid* to appropriately react to various situations. Therefore, to realize adaptive behavior the key issue is establishing a *soft* robot by designing an internal structure that adequately changes the response depending on the situation.

In our previous work (Aoi and Tsuchiya 2005), we designed a simple control system for a motor-driven biped robot by focusing on CPG characteristics, which had an internal structure composed of nonlinear oscillators, that generated robot kinematics and appropriately changed response

depending on the situation. Specifically, we generated robot kinematical motions using rhythmic signals from internal oscillators that responded to sensory signals and modulated the rhythmic signals and physical kinematics, resulting in three-dimensional, stable, adaptive straight walking. This means that a robot driven by this control system established adaptive straight walking not by calculating the physical kinematics in real-time based on an optimization criterion but by adequately changing the internal states depending on the situation. As a result of the changes in internal states, we clearly demonstrated that the modulation of walking rhythm plays an important role in generating adaptive straight walking.

In this paper, we extended this control system to obtain turning behavior to maintain a simple control system. Although this extension is straightforward and the control system remains simple, the robot achieves interesting adaptive behavior through interactions between the dynamics of its mechanical system, the internal structure, and the environment. To elucidate the mechanism that establishes adaptive turning behavior, we investigated the roles of the internal structure in its control system by focusing on walking rhythm. We used HOAP-1 (Fujitsu Automation Ltd., http://www.automation.fujitsu.com/en/), a biped robot introduced in Sect. 2, and analyzed its turning dynamics by considering that it consists of straight and curved walking and the transition between them, as mentioned above. Sections 3 and 4, respectively. Section 5 addresses the transition of walking patterns and turning. Sections 6 and 7 include discussion and conclusion, respectively.

2 Biped robot model

In this paper, we used HOAP-1 (Fujitsu Automation Ltd.), a biped robot shown in Fig. 2(a). Figure 2(b) shows its schematic model. The robot consists of a trunk, a pair of arms composed of four links, and a pair of legs composed of six links. Each link is connected to the others through a single degree of freedom rotational joint. Each joint has a proprioceptive sensor to monitor the joint state and is driven by a motor. Four touch sensors are attached to the sole of each foot. This robot has a three-axis gyrosensor used to monitor steady periodic motion. Its left and right legs are numbered Legs 1 and 2, respectively. Leg joints are numbered Joints $1 \ldots 6$ from the side of the trunk. Joints 1, 2, and 3 are hip joints, Joint 4 is a knee joint, and Joints 5 and 6 are ankle joints. Specifically, Joint 1 is a yaw joint, Joints 2 and 6 are roll joints, and Joints 3, 4, and 5 are pitch joints. The arms are numbered in a similar manner. To describe the configuration of the robot, we introduce angles θ_{Aj}^i and θ_{Lk}^i ($i = 1, 2$, $j = 1, \ldots, 4$, $k = 1, \ldots, 6$), which are rotation angles of Joint j of Arm i and Joint k of Leg i, respectively. Table 1 shows the physical parameters of the robot.

Fig. 2 Biped robot model: (**a**) and (**b**) show HOAP-1 (Fujitsu Automation Ltd.) and its schematic model [mm], respectively
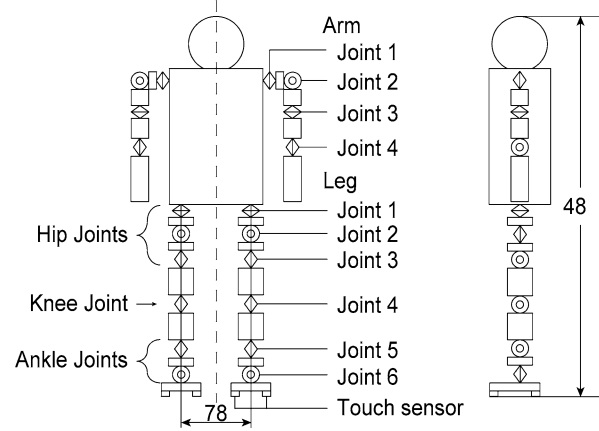
(a)　　　　　　　　　　　(b)

Table 1 Physical parameters of HOAP-1

Link	Mass [kg]	Length [m]
Trunk	2.34	0.20
Leg	1.32	0.28
Arm	0.43	0.22
Total	5.84	0.48

In numerical simulations, we derived equations of motion for this multi-linked rigid body system using Lagrangian equations in which the ground is modeled as a spring with a damper (Aoi and Tsuchiya 2005), and we used the fourth order Runge–Kutta method with step size 1 ms. Note that we verified the validity of the simulations by investigating such conditions as energy conservation, angular momentum conservation, and reaction forces from the ground under specific conditions.

In hardware experiments, we also used a host computer (Equivalent Pentium III 700 MHz, RT-Linux) to calculate the nominal joint trajectories and solve the phase dynamics of the oscillators, which we will explain below. The robot had power supply and Universal Serial Bus (USB) cables and received nominal joint trajectories as command signals by the USB cable from the host computer every 1 ms.

3 Adaptive behavior in straight walking

As mentioned in Sect.1.1, the turning behavior considered in this paper consists of straight walking, curved walking, and the transition between them. First, in this section we briefly describe the designed locomotion control system that obtained straight walking in our previous work (Aoi and Tsuchiya 2005).
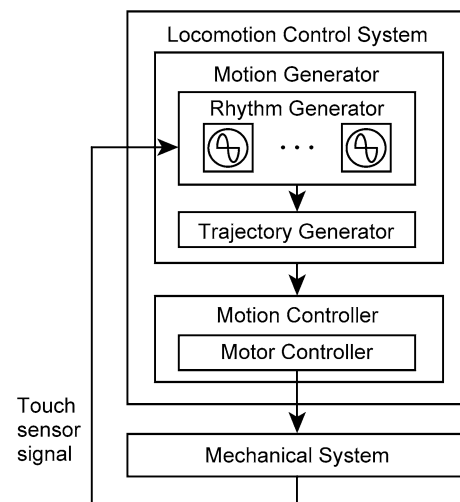
(a)
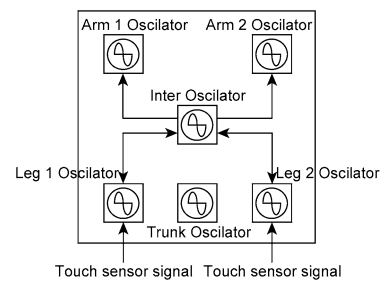
(b)

Fig. 3 Locomotion control system: (**a**) architecture of the locomotion control system and (**b**) rhythm generator

3.1 Locomotion control system for straight walking

The designed locomotion control system consists of a motion generator and controller (see Fig. 3(a)). The motion generator is composed of rhythm and trajectory generators. The rhythm generator has two types of oscillators: Motion and Inter (see Fig. 3(b)). The Motion oscillators consist of

Legs 1 and 2, Arms 1 and 2, and Trunk oscillators. The trajectory generator creates nominal trajectories of all joints using the phases of Motion oscillators, which are sent to the motion controller. The motion controller is comprised of motor controllers that manipulate the joint motions using local high-gain feedback control to follow the generated trajectories in the trajectory generator. Although we concisely describe the controller below, see (Aoi and Tsuchiya 2005) for further details.

3.1.1 Trajectory generator

As described above, the trajectory generator creates nominal trajectories of all joints based on the phases of Motion oscillators. Note that since our purpose was to elucidate how to achieve adaptive walking, we employed simple trajectories for the joints to avoid restricting application possibilities and to determine the essentials.

First, let ϕ_L^i, ϕ_A^i, ϕ_T, and ϕ_I ($i = 1, 2$) be the phases of Leg i, Arm i, Trunk, and Inter oscillators, respectively. The nominal trajectories of the arm joints are designed so that the arms oscillate relative to the trunk in the pitch plane. Specifically, nominal trajectories $\hat{\theta}_{Aj}^i$ ($i = 1, 2$, $j = 1, \ldots, 4$) of Joint j of Arm i are given by the functions of phase ϕ_A^i of Arm i oscillator and written by

$$
\begin{aligned}
\hat{\theta}_{A1}^i(\phi_A^i) &= \hat{A}\cos\phi_A^i, \\
\hat{\theta}_{A2}^i(\phi_A^i) &= 0, \\
\hat{\theta}_{A3}^i(\phi_A^i) &= 0, \\
\hat{\theta}_{A4}^i(\phi_A^i) &= \pi/2, \quad i = 1, 2,
\end{aligned}
\tag{1}
$$

where $\hat{A}$ is the nominal amplitude of the arm motion.

The nominal trajectories of the leg joints are determined by designing the nominal trajectory of the foot relative to the trunk. The nominal foot trajectory consists of the swing and stance phases, where the trunk has a constant nominal posture angle $\hat{C}$ with respect to the line that involves anterior extreme position (AEP) and posterior extreme position (PEP) (see Fig. 4). The former is composed of a simple closed curve that includes points AEP and PEP. This trajectory starts from point PEP and continues until the leg touches the ground. The latter consists of a straight line from the foot landing position (LP) to point PEP. Therefore, this trajectory depends on the timing of the foot contact with the ground in each step cycle. These two nominal trajectories of the foot give nominal trajectories $\hat{\theta}_{Lj}^i$ ($i = 1, 2$, $j = 3, 4, 5$) of Joint j (hip, knee, and ankle pitch joints) of Leg i by the functions of phase ϕ_L^i of Leg i oscillator written by $\hat{\theta}_{Lj}^i(\phi_L^i)$, where we use $\phi_L^i = 0(2\pi)$ at point PEP and $\phi_L^i = \hat{\phi}_{AEP}$ at point AEP. Note that nominal stride $\hat{S}$ is given by the distance between points AEP and PEP, and duty factor $\hat{\beta}$ is
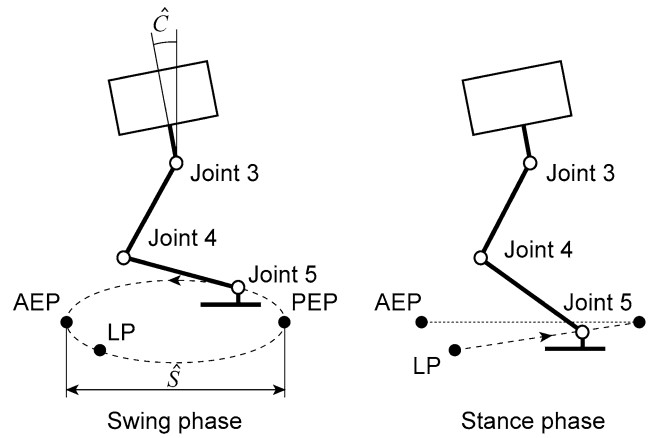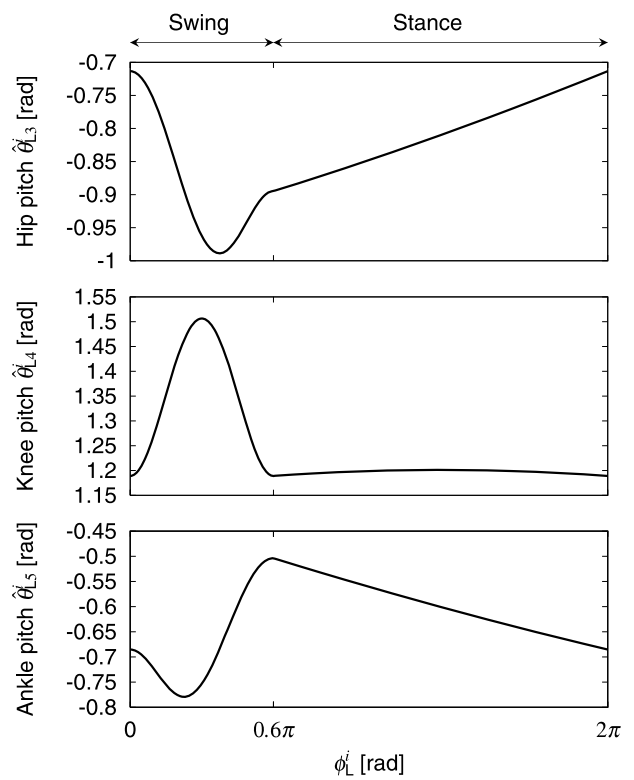

Fig. 4 Nominal foot trajectory

Fig. 5 Nominal trajectories $\hat{\theta}_{Lj}^i$ ($i = 1, 2$, $j = 3, 4, 5$) with respect to phase ϕ_L^i of Leg i oscillator where point LP equals point AEP and $\hat{\beta} = 0.7$, where $0 \leq \phi_L^i < 0.6\pi$ indicates the swing phase and $0.6\pi \leq \phi_L^i < 2\pi$ corresponds to the stance phase

given by the ratio between the nominal stance phase and step cycle durations. Figure 5 illustrates nominal trajectories $\hat{\theta}_{Lj}^i$ ($i = 1, 2$, $j = 3, 4, 5$) with respect to phase ϕ_L^i of Leg i oscillator where point LP is equal to point AEP, using the following parameters: $\hat{S} = 3$ cm, $\hat{\beta} = 0.7$, and $\hat{C} = 12°$, where $\hat{\phi}_{AEP} = 0.6\pi$, $0 \leq \phi_L^i < \hat{\phi}_{AEP}$ indicates the swing phase, and $\hat{\phi}_{AEP} \leq \phi_L^i < 2\pi$ corresponds to the stance phase.

The nominal trajectories of the arm and leg joints described above are only considered on the pitch plane. However, since the biped robot walks in three-dimensional space, it might topple laterally especially when only supported by one leg. Therefore, the nominal trajectories of the hip and ankle roll joints are designed so that the roll motion of the trunk achieves periodic motion whose cycle resembles the step cycle and compensates for lateral motion, preventing the robot from falling laterally. Thus, nominal trajectories $\hat{\theta}^i_{Lj}$ ($i = 1, 2$, $j = 2, 6$) of Joint j (hip and ankle roll joints) of Leg i are given by the functions of phase ϕ_T of Trunk oscillator and written by

$$
\begin{aligned}
\hat{\theta}^i_{L2}(\phi_T) &= \hat{B}\cos(\phi_T + \hat{\psi}) - (-1)^i \hat{\Delta}, \\
\hat{\theta}^i_{L6}(\phi_T) &= -\hat{B}\cos(\phi_T + \hat{\psi}) + (-1)^i \hat{\Delta}, \quad i = 1, 2,
\end{aligned}
\tag{2}
$$

where $\hat{B}$ and $\hat{\psi}$ are the nominal amplitude and phase of this roll motion and $\hat{\Delta}$ is the nominal bias angle to avoid a collision between the legs. Since we don't consider yaw motion in straight walking, we use $\hat{\theta}^i_{L1} = 0$ ($i = 1, 2$) for Joint 1 (hip yaw joint) of Leg i.

3.1.2 Rhythm generator and sensory feedback

In the rhythm generator, Motion and Inter oscillators generate rhythmic behavior based on the following phase dynamics:

$$
\begin{aligned}
\dot{\phi}_I &= \hat{\omega} + g_{1I}, \\
\dot{\phi}_T &= \hat{\omega} + g_{1T}, \\
\dot{\phi}^i_A &= \hat{\omega} + g^i_{1A}, \quad i = 1, 2, \\
\dot{\phi}^i_L &= \hat{\omega} + g^i_{1L} + g^i_{2L}, \quad i = 1, 2,
\end{aligned}
\tag{3}
$$

where g_{1I}, g_{1T}, g^i_{1A}, and g^i_{1L} ($i = 1, 2$) are functions regarding the nominal phase relationship shown below, g^i_{2L} ($i = 1, 2$) is a function arising from the sensory feedback given below, and $\hat{\omega}$ is the nominal angular velocity of each oscillator obtained by

$$
\hat{\omega} = 2\pi \frac{1 - \hat{\beta}}{\hat{T}_{Sw}}
\tag{4}
$$

where $\hat{T}_{Sw}$ is the nominal swing phase duration.

To establish stable bipedal walking, the essential problem is coordination of the joint motions: interlimb coordination is the key. For example, both legs must move out of phase to keep the robot from falling over. Since the nominal joint trajectories for the trunk and limbs are designed in the previous section by oscillator phases, interlimb coordination is given by the phase relation, that is, the phase differences between oscillators. Functions g_{1I}, g_{1T}, g^i_{1A}, and g^i_{1L} in (3) deal with interlimb coordination and are given by the phase

differences between the oscillators based on Inter oscillator, written by

$$
\begin{aligned}
g_{1I} &= -\sum_{i=1}^{2} K_L \sin(\phi_I - \phi^i_L + (-1)^i \pi/2), \\
g_{1T} &= -K_T \sin(\phi_T - \phi_I), \\
g^i_{1A} &= -K_A \sin(\phi^i_A - \phi_I + (-1)^i \pi/2), \quad i = 1, 2, \\
g^i_{1L} &= -K_L \sin(\phi^i_L - \phi_I - (-1)^i \pi/2), \quad i = 1, 2,
\end{aligned}
\tag{5}
$$

where the nominal phase relations are given so that both the arms and legs move out of phase and one arm and the contralateral leg move in phase and K_L, K_A, and K_T are gain constants.

As well as interlimb coordination, modulation of walking rhythm is an important factor to generate walking. As mentioned in Sect. 1.2, CPGs in animals modulate neural activity in response to sensory information and achieve robust walking. Function $g^{(i)}_{2L}$ modulates walking rhythm through phase modulation of the leg oscillators based on sensory signals. Specifically, when the foot of Leg i lands on the ground, Leg i oscillator receives a feedback signal from the touch sensor ($i = 1, 2$). Instantly, phase ϕ^i_L of Leg i oscillator is reset to nominal value $\hat{\phi}_{AEP}$ from value ϕ^i_{land} at the landing. Therefore, function g^i_{2L} is written by

$$
g^i_{2L} = (\hat{\phi}_{AEP} - \phi^i_{land})\delta(t - t^i_{land}), \quad i = 1, 2,
\tag{6}
$$

where $\hat{\phi}_{AEP} = 2\pi(1 - \hat{\beta})$, t^i_{land} is the time when the foot of Leg i lands on the ground ($i = 1, 2$), and $\delta(\cdot)$ denotes Dirac's delta function. Note that touch sensor signals modulate not only the walking rhythm but also the robot joint motions, as described in Sect. 3.1.1. Some studies employed phase resetting and demonstrated its significant role in stabilizing the walking motion of biped robots (Nakanishi et al. 2004, 2006).

Using this control system, the robot is driven by rhythmic signals from the oscillators and achieves adaptive straight walking by adequately modulating walking rhythm depending on sensory signals verified by numerical simulations and hardware experiments that employed environmental changes and disturbances.

3.2 Limit cycle of straight walking

In this section, we show the obtained limit cycle of straight walking. In particular, throughout this paper we investigate two types of locomotion speed, low and moderate. When humans change walking speed, the swing phase duration remains constant, and the duty factor chiefly changes (Orlovsky et al. 1999; Nilsson and Thorstensson 1989). Therefore, we use nominal swing phase duration $\hat{T}_{Sw}$ and

stride $\hat{S}$ as 0.3 s and 3 cm, respectively, and employ nominal duty factor $\hat{\beta}$ as 0.7 for slow speed and 0.5 for moderate speed. It follows that the nominal step cycle and locomotion speed become 1.0 s and 4.3 cm/s for slow speed and 0.6 s and 10 cm/s for moderate speed. The other parameters in the control system are set as follows: $K_T = 5$, $K_A = 5$, $K_L = 10$, $\hat{A} = 10°$, $\hat{\psi} = -150°$, $\hat{\Delta} = 2°$, $\hat{B} = 7°$ (for $\hat{\beta} = 0.7$), $2°$ (for $\hat{\beta} = 0.5$), and $\hat{C} = 12°$. Note that these parameters are determined so that the robot obtains stable straight walking in numerical simulations, verified by using a Poincaré map, and then we apply them to hardware experiments.

Figures 6(1) and (2) show the roll and pitch motions of straight walking, respectively, obtained by numerical simulations and hardware experiments. Specifically, A and B depict the time-series data of angular velocity at low ($\hat{\beta} = 0.7$) and moderate speeds ($\hat{\beta} = 0.5$), respectively. C and D show the limit cycle of straight walking at low ($\hat{\beta} = 0.7$) and moderate speeds ($\hat{\beta} = 0.5$), respectively, where we averaged these motions in hardware experiments because they slightly fluctuated. Since we used a three-axis gyrosensor to monitor these motions in the experiments, angle data have more error between the numerical and hardware results than angular rate data. Although such errors exist, they have almost similar results.

4 Adaptive behavior in curved walking

4.1 Curved walking strategy

In this section, we discuss curved walking. As mentioned in Sect. 1.1, a model-based approach is often used to accomplish various motions. However, elaborate computations are required, as is precise modeling of both the robot and the environment, which restricts the possibility of attaining adaptability and robustness. Such an approach is not suitable, since the aim of this paper is to elucidate how to establish adaptive walking through interactions between the dynamics of a robot's mechanical system, its internal oscillators, and the environment, as achieved in straight walking. Therefore, to obtain curved walking and clearly investigate it, we slightly extend the locomotion control system designed and described in the last section and retain a simple control system.

To design a strategy for robot curved walking, we refer to human curved walking. In human curved walking, walking direction only changes when the external foot is in contact with the ground, and straight walking is sustained when the internal foot has such contact; that is, curved walking is comprised of successive quick turnings and straight walkings (Courtine and Schieppati 2003a; Imai et al. 2001). Specifically, such turning motions are accomplished by rotating the trunk using the hips and then stepping in the

new direction (Hase and Stein 1999; Hollands et al. 2001). Therefore, the following procedure between two successive onsets of the swing phase of the internal foot is considered the basic actions of robot curved walking:

1. When the internal foot is in the swing phase, the trunk and internal leg are rotated in the new direction by manipulating the hip yaw joint (Joint 1) of the external leg.
2. When the internal foot touches the ground and becomes the stance phase and when the external leg is in the swing phase, the external leg is also rotated in the new direction by manipulating the hip yaw joint of the external leg.

These basic actions mean that the robot simply changes the stepping direction of the swing leg using the hip yaw joint, as shown in Fig. 7. In particular, the robot uses the hip yaw joint of its right leg to curve to the left depending on the phase of the left leg and uses the hip yaw joint of its left leg to curve to the right depending on the phase of the right leg. Note that the robot did not actively use the hip yaw joint in straight walking, as described in Sect. 3.1.1. Also note that in curved walking the robot uses the other joints in the same way as straight walking.

To ascertain the new direction during curved walking, we introduce parameter Y^i that determines the turning angle per step of Leg i ($i = 1, 2$), where $Y^1 > 0$ and $Y^2 > 0$ indicate curved walking to the right and left, respectively. Based on the basic actions of curved walking, nominal trajectory $\hat{\theta}_{L1}^i$ ($i = 1, 2$) of Joint 1 (hip yaw joint) of Leg i is designed using phase ϕ_T of Trunk oscillator by

$$
\hat{\theta}_{L1}^i(\phi_T) = \begin{cases}
\frac{(-1)^i Y^i}{2}\{1 - \cos\frac{\phi_T - (-1)^i \pi/2}{\hat{\phi}_{AEP}/\pi}\}, \\
\quad 0 \le \phi_T - (-1)^i \pi/2 \pmod{2\pi} < \hat{\phi}_{AEP}, \\
\frac{(-1)^i Y^i}{2}\{1 - \cos\frac{2\pi - (\phi_T - (-1)^i \pi/2)}{2 - \hat{\phi}_{AEP}/\pi}\}, \\
\quad \hat{\phi}_{AEP} \le \phi_T - (-1)^i \pi/2 \pmod{2\pi} < 2\pi, \\
\end{cases}
$$
$$
i = 1, 2 \tag{7}
$$

where $a \pmod{b}$ indicates the remainder when a is divided by b. Note that $Y^1 = Y^2 = 0°$ implies straight walking, and the robot is not allowed to implement a change of walking direction with $Y^1 > 0°$ and $Y^2 > 0°$. This equation indicates the following: when the robot curves to the left ($Y^2 > 0$), it uses hip yaw joint $\hat{\theta}_{L1}^2$ of the right leg depending on the phase of the left leg; since the phase of Leg 1 oscillator is written as $\phi_T - \pi/2 \pmod{2\pi}$ from the phase relation described in Sect. 3.1.2, $0 \le \phi_T - \pi/2 \pmod{2\pi} < \hat{\phi}_{AEP}$ indicates the swing phase of the left leg and $\hat{\phi}_{AEP} \le \phi_T - \pi/2 \pmod{2\pi} < 2\pi$ implies the stance phase of the left leg; during the swing phase of the left leg, the robot faces the left by manipulating the hip yaw joint of the right leg following the upper equation of (7); dur-

Fig. 6 Periodic states in
straight walking, obtained by
numerical simulations and
hardware experiments. (**1**) and
(**2**) show the roll and pitch
motions, respectively. **A** and **B**
display the time-series data of
the angular velocity at low
($\hat{\beta} = 0.7$) and moderate speeds
($\hat{\beta} = 0.5$), respectively. **C** and **D**
show limit cycles of straight
walking at low ($\hat{\beta} = 0.7$) and
moderate speeds ($\hat{\beta} = 0.5$),
respectively
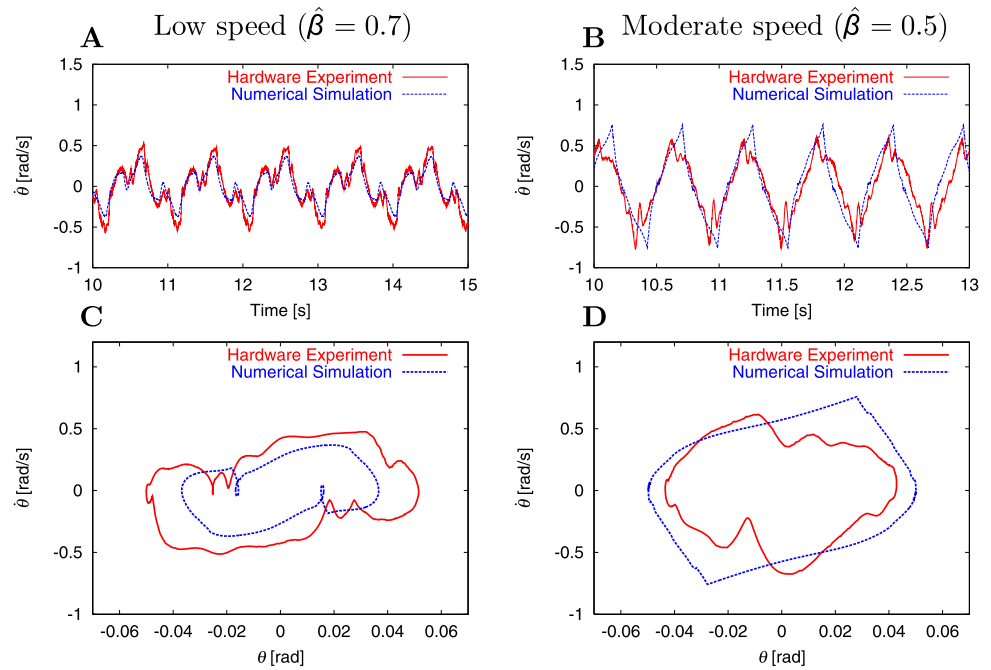
(1) roll motion
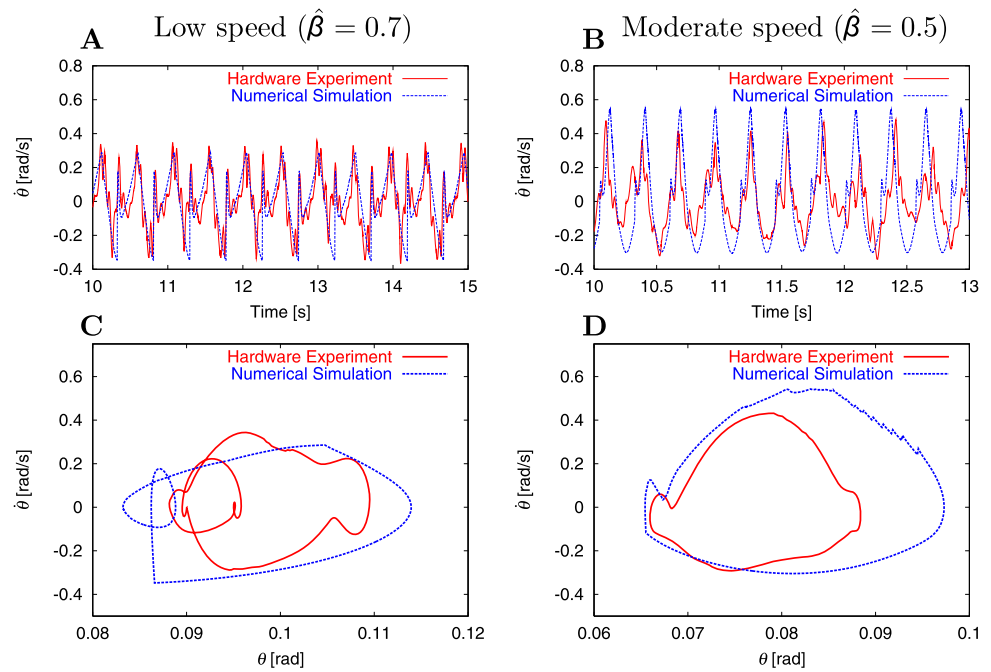
(2) pitch motion

ing the stance phase of the left leg, the robot rotates its right leg by using the hip yaw joint of the right leg in the new direction following the lower equation of (7); when the robot curves to the right ($Y^1 > 0$), it follows a similar procedure.

Since nominal locomotion speed is given by $\hat{S}(1 - \hat{\beta})/(\hat{\beta}\hat{T}_{Sw})$ (Aoi and Tsuchiya [2005](#)), nominal curved radius

$\hat{R}^i$ becomes equivalent to

$$\hat{R}^i = \frac{360°}{Y^i} \frac{\hat{S}}{2\pi\hat{\beta}}, \quad i = 1, 2 \tag{8}$$

where $\hat{R}^1$ and $\hat{R}^2$ indicate the radius during curved walking to the right and left, respectively.

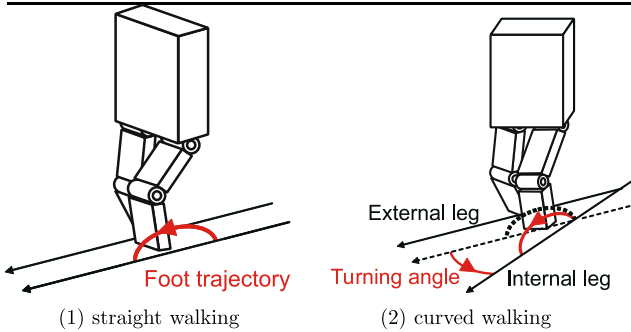(1) straight walking   (2) curved walking

Fig. 7 Stepping direction of legs in straight and curved walking

Using this simple strategy, we investigate curved walking of the robot by the numerical simulations and hardware experiments listed below.

4.2 Limit cycle of curved walking

The proposed strategy for curved walking merely changes the stepping direction of the swing leg. Although this is not designed for the robot to achieve stable curved walking, this control system does establish stable curved walking. In this section, we first show the obtained limit cycle of curved walking and investigate the mechanism for establishing it in the next section.

Figures 8(1) and (2) show the roll and pitch motions of curved walking, respectively, obtained by numerical simulations and hardware experiments, where we used the following parameters: $Y^1 = 0°$ and $Y^2 = 15°$, which mean the robot's curved walking to the left with $15°$ of turning angle per step. Specifically, A and B display the profile of angular velocity at low ($\hat{\beta} = 0.7$) and moderate speeds ($\hat{\beta} = 0.5$), respectively, and C and D show the phase diagram at low ($\hat{\beta} = 0.7$) and moderate speeds ($\hat{\beta} = 0.5$), respectively. These figures verify that numerical simulations attain the limit cycle of curved walking and that hardware experiments accomplish periodic curved walking. Although errors exist between the numerical and hardware results, they have almost similar results. Note that the limit cycle obtained in the numerical simulations was also verified using a Poincaré map (for details see Aoi and Tsuchiya 2005).

Figures 9(1) and (2) depict the trunk trajectory projected on the ground during curved walking at low ($\hat{\beta} = 0.7$) and moderate speeds ($\hat{\beta} = 0.5$), respectively, obtained by numerical simulations and nominal curved radius $\hat{R}$ in (8). Although errors remain between the obtained and nominal trajectories, the robot adequately achieves curved walking without a feedback controller to keep it on the nominal trajectory.

### 4.3 Adaptive curved walking due to sensory feedback

4.3.1 Investigation based on turning angle

In this section, we examine how this control system establishes stable curved walking. As mentioned in Sect. 4.1, turning angles $Y^1 = Y^2 = 0°$ indicate straight walking. Our previous work (Aoi and Tsuchiya 2005) investigated how this control system accomplishes stable straight walking, revealing that adequate modulation of walking rhythm in response to sensory information plays an important role in generating stable and adaptive straight walking. Therefore, we focus on these parameters and examine the behavior in various kinds of curved walking.

At the beginning of the numerical simulations and hardware experiments, turning angles Y^1 and Y^2 were both set to $0°$: the robot walks straight. Then, we gradually increased turning angle Y^2 to induce curved walking to the left while the robot is walking. Figures 10(1) and (2) show the results at low ($\hat{\beta} = 0.7$) and moderate speeds ($\hat{\beta} = 0.5$), respectively, obtained by numerical simulations and hardware experiments. Specifically, A and B show the resultant duty factors and step cycles, respectively, of the left and right legs versus turning angle Y^2, where resultant duty factor β^i ($i = 1, 2$) of Leg i is calculated by the ratio between the resultant stance phase and step cycle durations. These figures indicate that an increase in turning angle decreases resultant duty factor β^1 of the left leg (internal leg) and increases resultant duty factor β^2 of the right leg (external leg), while the step cycle remains almost unchanged. When turning angle Y^2 exceeded $20°$ at low speed ($\hat{\beta} = 0.7$) and $40°$ at moderate speed ($\hat{\beta} = 0.5$) in hardware experiments, we could not achieve reasonable data. Figures 11(1) and (2) show comparisons of the curved radius with respect to turning angle Y^2 between the numerical and experimental results and nominal value in (8) at low ($\hat{\beta} = 0.7$) and moderate speeds ($\hat{\beta} = 0.5$), respectively, calculated by trunk trajectories projected on the ground in numerical simulations and by foot positions in hardware experiments. Although discrepancy exists between the simulation and experimental results and the nominal value especially as the turning angle decreases, the robot establishes appropriate curved walking without a feedback controller that helps the robot follow the nominal trajectory.

In straight walking, the robot has kinematically identical periodic motions between the left and right limbs and can walk straight, although the motion phases differ almost half a step cycle. In that sense, the robot's straight walking motions are kinematically symmetric between the right and left limbs. On the other hand, in curved walking, the robot has kinematically different periodic motions between the left and right limbs and walks to the right or left. For example, in this paper, this corresponds to the mo-

Fig. 8 Periodic states in curved walking, obtained by numerical simulations and hardware experiments. (**1**) and (**2**) show results at low ($\hat{\beta} = 0.7$) and moderate speeds ($\hat{\beta} = 0.5$), respectively. **A** and **B** display the time-series data of angular velocity with respect to roll and pitch motions, respectively. **C** and **D** show the limit cycle of curved walking with respect to roll and pitch motions, respectively
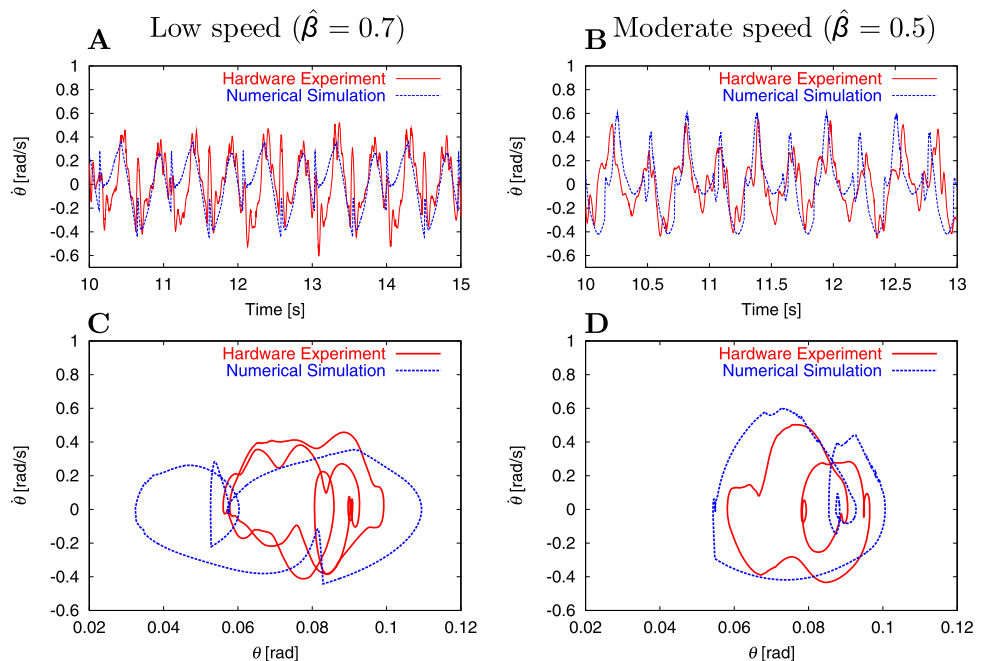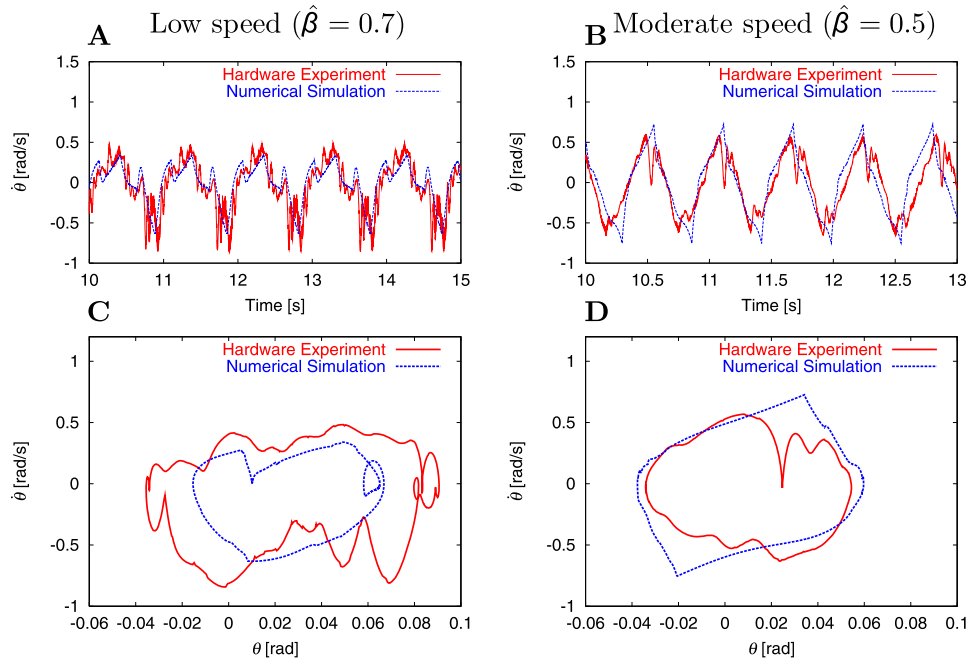
tions of the hip yaw joints, as designed in (7), meaning that the robot motions of curved walking are kinematically asymmetric between the right and left limbs. Such asymmetry, which is crucial in the dynamics of curved walking, generally lowers walking stability. Therefore, to achieve stable curved walking, a mechanism is necessary to compensate for the decreased stability caused by asymmetry.

Asymmetry in curved walking both kinematically and dynamically influences walking. Its most crucial effect is on the timing of the foot contact with the ground. In straight walking, the foot contacts of the right and left legs occur almost out of phase. However, in curved walking, asymmetry results in timing changes. Therefore, swing and stance phase durations are almost identical between the legs in straight walking and different in curved walking. As shown

Fig. 9 Trunk trajectory during curved walking. (**1**) and (**2**) show results at low ($\hat{\beta} = 0.7$) and moderate speeds ($\hat{\beta} = 0.5$), respectively
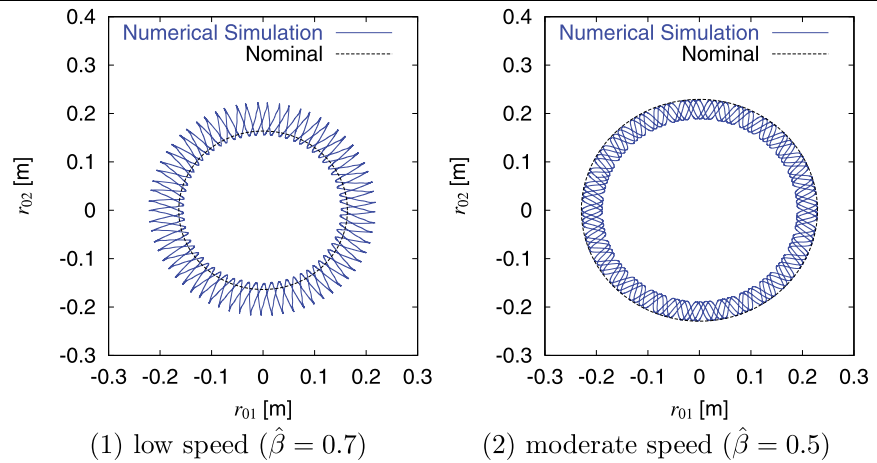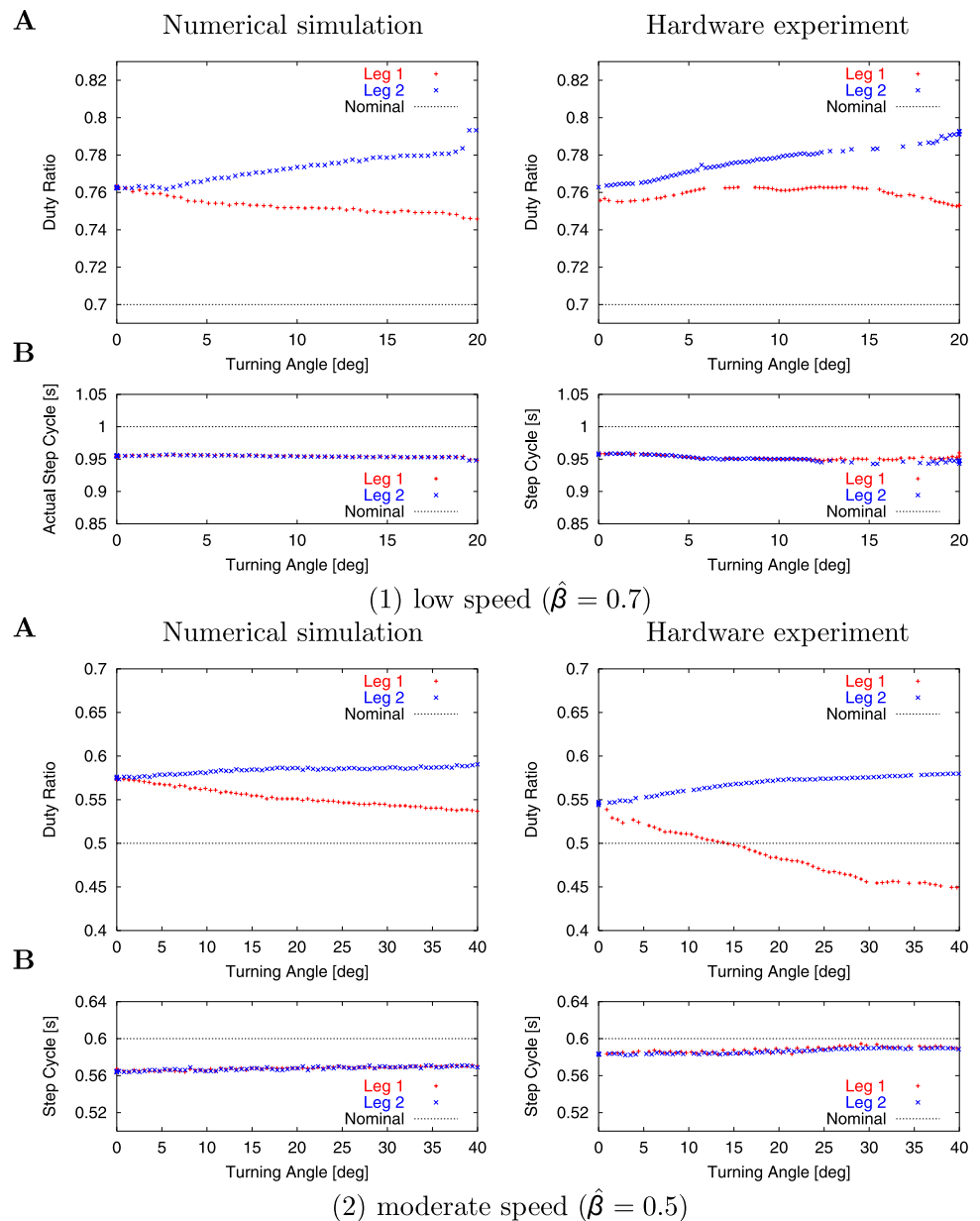

(1) low speed ($\hat{\beta} = 0.7$)   (2) moderate speed ($\hat{\beta} = 0.5$)

Fig. 10 Curved walking with respect to turning angle per step Y^2 at (**1**) low speed ($\hat{\beta} = 0.7$) and (**2**) moderate speed ($\hat{\beta} = 0.5$). **A** and **B** show resultant duty factor and step cycles, respectively, versus turning angle per step Y^2. *Left and right sides of figures* are obtained by numerical simulations and hardware experiments, respectively

(1) low speed ($\hat{\beta} = 0.7$)

(2) moderate speed ($\hat{\beta} = 0.5$)

Fig. 11 Curved radius with respect to turning angle Y^2 between numerical and experimental results and nominal value at (**1**) low ($\hat{\beta} = 0.7$) and (**2**) moderate speeds ($\hat{\beta} = 0.5$)

(1) low speed ($\hat{\beta} = 0.7$)   (2) moderate speed ($\hat{\beta} = 0.5$)
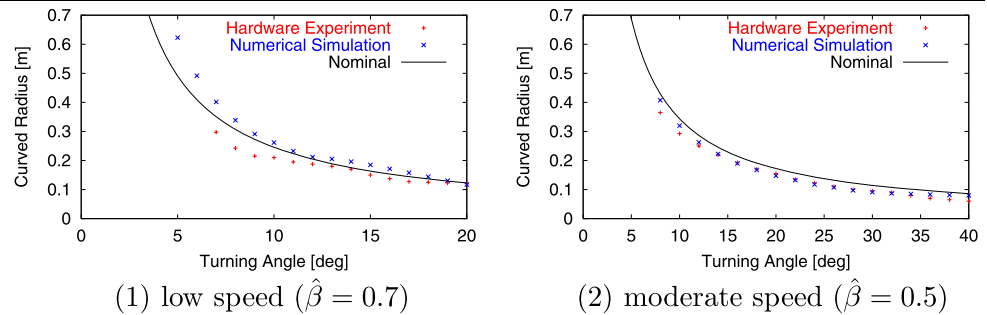
in Figs. 10(1) and (2)A, this leads to identical duty factors in straight walking ($Y^2 = 0°$) and different duty factors in curved walking ($Y^2 > 0°$) between the legs.

Based on foot contacts, this control system modulates walking rhythm by resetting oscillator phases, as mentioned in Sect. 3.1.2. It also modulates joint motions by switching the foot trajectories from the swing to the stance phase, as described in Sect. 3.1.1. Note that this control system has separate oscillators for the legs, namely, Leg 1 and Leg 2 oscillators, which directly modulate their own phases and corresponding joint motions in response to the foot contacts of the corresponding leg. Therefore, this control system can generate different rhythms between the legs.

The robot has difficulty establishing stable walking when the right and left legs have different rhythms. In this control system, the oscillators have interaction (5), as mentioned in Sect. 3.1.2, that attempts to maintain the phase difference between Leg oscillators as out of phase. These interactions, in fact, realize almost the same rhythm between the legs, despite the shift of difference in foot contact timing between the legs from out of phase. Thus, in such walking that has asymmetry as curved walking, this control system compensates for the decreased stability caused by asymmetry by modulating the phase and timing of robot motions in each limb, while generating the same rhythm in the robot motions through interactions between oscillators. Figure 10 actually suggests this point, which we investigate in the next section.

4.3.2 Investigation of phase modulation

Courtine and Schieppati (2003b) studied human turning and revealed not only spacial asymmetry between leg motions but also temporal asymmetry. Specifically, when human walking changes from straight to curved, the duty factor of the external leg decreases due to a reduction in the stance phase duration and an increase in the swing phase duration despite almost no change in the step cycle duration; the opposite occurs in the internal leg. This feature resembles the results obtained in Fig. 10. Furthermore, Courtine and Schieppati found that although the phase lag between leg motions in human straight walking is almost out of phase, in human curved walking it shifts from out of phase. As

pointed it out in the previous section, to examine the details of this point we introduce phase lag $\Delta\phi$, referring to their definition,

$$\Delta\phi = 360° \times \Delta t / T \qquad (9)$$

where Δt indicates the difference between the time when the external foot lands on the ground and the time halfway between two successive internal foot landings and T indicates the step cycle duration of the internal leg. Note that phase lag $\Delta\phi$ is different from phase lag $\phi_L^1 - \phi_L^2$ calculated from the phases of Leg oscillators, $\Delta\phi = 0°$ indicates that the internal and external legs are out of phase, and $\Delta\phi > 0°$ implies a phase lag of the external leg with respect to the internal leg. Figures 12(1) and (2) show phase lag $\Delta\phi$ for turning angle per step Y^2 at low ($\hat{\beta} = 0.7$) and moderate speeds ($\hat{\beta} = 0.5$), respectively, obtained by numerical simulations and hardware experiments. Although errors exist between numerical and hardware results, they have similar properties. These figures suggest that although in straight walking ($Y^2 = 0°$), the phase lag between the legs is out of phase, asymmetry from the increase in the turning angle increases the phase lag, similar to human walking.

As described in Sect. 3.1.2, the phases of Leg oscillators are reset based on the timing of foot contact. Therefore, phase lag due to the timing of foot contact causes the phase difference to fluctuate between Leg oscillators. On the other hand, interaction between Leg oscillators given in (5) attempts to maintain the phase difference of Leg oscillators as out of phase, actually resulting in the same rhythm between the legs, as mentioned in the previous section. Although phase lag lowers the stability of straight walking, the temporal asymmetry associated with it helps compensate for the spacial asymmetry arising from the kinematical differences between leg motions for achieving adaptive curved walking.

5 Transition of walking patterns and turning

In this section, we analyze robot turning. As explained in Sect. 1.1, turning is achieved by the transition between the straight and curved walking. Furthermore, as mentioned in

Fig. 12 Phase lag between leg motions for turning angle per step Y^2 at (**1**) low ($\hat{\beta} = 0.7$) and (**2**) moderate speeds ($\hat{\beta} = 0.5$). *Left and right sides of the figures* are obtained by numerical simulations and hardware experiments, respectively

Numerical simulation — Hardware experiment

(1) low speed ($\hat{\beta} = 0.7$)

Numerical simulation — Hardware experiment

(2) moderate speed ($\hat{\beta} = 0.5$)
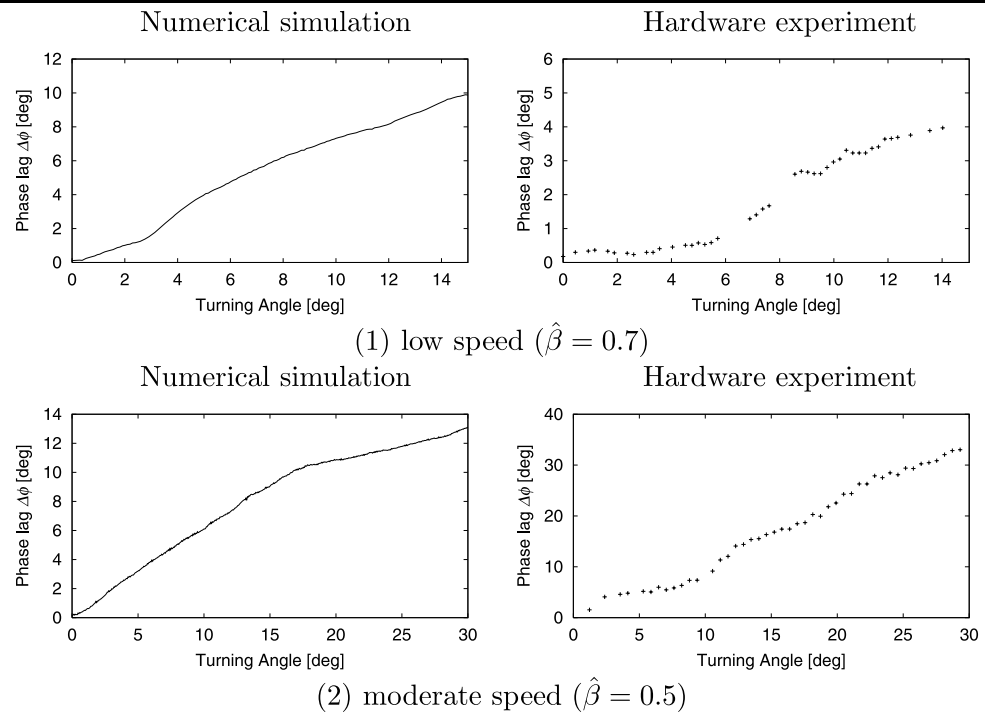
Sect. 4.1, the difference between straight and curved walking of robot motions is only turning angle Y^i ($i = 1, 2$). Therefore, the robot can kinematically change its walking pattern using turning angle Y^i.

As described in Sect. 1.1, since steady walking attains stable limit cycle in the state space of the robot, the transition between these walking patterns is identical to the transition between these limit cycles. Since different periodic motions have different limit cycles, as shown in Figs. 6 and 8, their transition is not necessarily confirmed as completed. However, note that when the robot changes its walking pattern, if its state is inside the basin of attraction of the limit cycle of the walking pattern to be changed, the transition will be accomplished (see Fig. 13). On the other hand, if the state is outside the basin of attraction, it will fail. Therefore, we can verify that the robot achieves a transition of walking patterns and turning by investigating the basin of attraction of the limit cycles of the walking patterns.

Since this control system established limit cycles of straight walking in Sect. 3.2 and curved walking in Sect. 4.2, as verified by a Poincaré map, these limit cycles are at least locally stable and have basins of attraction in the linear region around the trajectories. However, at the moment of the implementation of the walking pattern's change, it is not verified that the state on the limit cycle of the *initial* walking pattern is inside the basin of attraction of the limit cycle of the *changed* walking pattern. Thus, for verification, we need to determine if the state is inside the basin of attraction of the limit cycle of the changed walking pattern when the robot changes walking patterns.
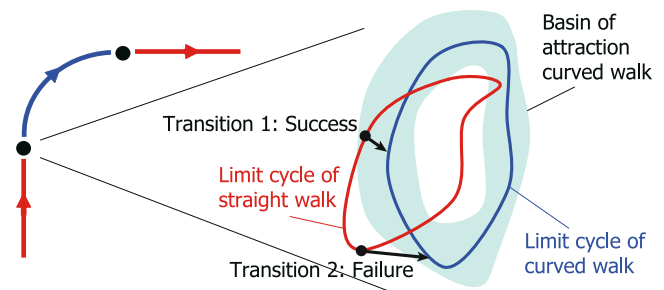

Fig. 13 Schematic of transition from limit cycle of straight walking to limit cycle of curved walking. Transition 1: Since the state on the limit cycle of straight walking is inside the basin of attraction of the limit cycle of curved walking at moment of implementation of the change in walking pattern, this transition will be achieved. Transition 2: Since the state is outside the basin of attraction, this transition will fail

Such a thorough investigation of the basin of attraction will help reveal the usefulness of this control system for the transition of walking patterns and robot turning. In particular, we will examine it based on numerical simulations in Sect. 5.1 and verify that the robot actually achieves transitions and turning based on hardware experiments in Sect. 5.2.

5.1 Investigation based on basin of attraction of the limit cycle

In this section, we investigate the basin of attraction of the limit cycle of straight and curved walking based on numerical simulations. Since roll and pitch motions are crucial in three-dimensional walking, we focus on them. In general,

these motions influence each other. However, we analyze them separately since they are relatively small, as shown in Figs. 6 and 8. To examine whether the robot establishes a transition of walking patterns, we especially need to examine the basin of attraction for these motions *at the moment of the implementation of the change in the walking pattern*. In other words, we must investigate how robust this control system is against disturbances at the moment.

In particular, we study the transition from straight to curved to the left and the inverse. In such transitions, we set turning angle per step Y^1 of the left leg to $0°$ and only change the turning angle per step Y^2 of the right leg. Specifically, we change it from $0°$ to $15°$ in the transition from straight to curved to the left and from $15°$ to $0°$ in the inverse. We implement the changes when $\phi_T = \pi/2$ is satisfied by following the starting point in the step cycle of curved walking to the left in the basic actions of curved walking, as defined in Sect. 4.1. The timing of the implementation of this change is called the transition point.

First, we show that the robot actually achieves these transitions. Figures 14 and 15 depict robot states in the transition from straight to curved and from curved to straight, respectively, obtained by numerical simulations, where (1) and (2) display the roll and pitch motions, respectively. Specifically, A and B depict the time-series data of angular velocity at low ($\hat{\beta} = 0.7$) and moderate speeds ($\hat{\beta} = 0.5$), respectively, and C and D show the phase diagram at low ($\hat{\beta} = 0.7$) and moderate speeds ($\hat{\beta} = 0.5$), respectively, which imply the transition from the limit cycle of the initial walking pattern to the limit cycle of the changed walking pattern. Since these transitions are successfully accomplished, the results mean that the states of the limit cycle of the initial walking pattern at the transition point are inside the basin of attraction of the limit cycle of the changed walking pattern. Therefore, it is verified that the robot can accomplish the transition if it establishes the limit cycle of the initial walking pattern before the transition.

Next, we attempt to achieve the basin of attraction to examine if the robot obtains the transition when the robot states are not on the limit cycle of the initial walking pattern by disturbing the pitch or roll motion at the transition point and determining if the trajectory of these motions converges at the limit cycle of the changed walking pattern obtained in cases without disturbance. Specifically, when the robot establishes a limit cycle of the initial walking pattern and when ϕ_T becomes $\pi/2$, we change the walking pattern by changing turning angle per step Y^2, and we also add disturbance to the roll or pitch motion. Figures 16 and 17 show the basin of attraction of the limit cycle of the changed walking pattern at the transition point with respect to the roll and pitch motions in transition from straight to curved and from curved to straight, respectively, obtained by numerical simulations, where (1) and (2) display the transition at low ($\hat{\beta} = 0.7$) and

moderate speeds ($\hat{\beta} = 0.5$), respectively. These figures reveal that this control system has a large basin of attraction for the roll and pitch motions, and they also verify the effectiveness of the control system in the transition of walking patterns and turning motion. The obtained basins of attraction with respect to the transitions from straight to curved and from curved to straight have similar size and shape, suggesting that the control system has similar characteristics and performance between straight and curved walking.

5.2 Experimental verification

In this section, we investigate whether the robot actually achieves transition of walking patterns between straight and curved walking and turning by hardware experiments. At the beginning of the experiments, the robot walks straight with $Y^1 = 0°$ and $Y^2 = 0°$. Then, it begins to curve to the left with $Y^1 = 0°$ and $Y^2 = 15°$. Next, the robot's motion returns to straight walking with $Y^1 = 0°$ and $Y^2 = 0°$ and then changes to curved walking to the right with $Y^1 = 15°$ and $Y^2 = 0°$. Finally, the robot walks straight again with $Y^1 = 0°$ and $Y^2 = 0°$. In this case, by regulating the number of steps for each walking pattern, the robot walks in a figure eight (see Fig. 18A). Figures 18B(1) and (2) show the resultant duty factors of left leg β^1 and right leg β^2 for the step numbers at low ($\hat{\beta} = 0.7$) and moderate speeds ($\hat{\beta} = 0.5$), respectively. These figures verify that the duty factors of the legs vary based on walking patterns, as obtained in Fig. 10, and that the transition of walking patterns is smoothly accomplished. Videos of these experiments are available at http://control.kuaero.kyoto-u.ac.jp/member/aoi/.

6 Discussion

6.1 Adaptability due to rhythm and phase modulations

In neurophysiology, many studies have been conducted to elucidate the control mechanism in animal walking and have revealed that rhythm and muscle tone controls play important roles in generating adaptive walking (Mori 1987; Rossignol 1996; Takakusaki et al. 2003, 2004). However, most robots are manipulated by motors that have completely different actuators from animal muscles. In motor control, robot joints are generally controlled so that they follow the desired trajectories using local high-gain feedback control. That is, robot motions are kinematically determined, and it is difficult for motors to achieve such a control system as animals. However, robots can easily modulate walking rhythm by manipulating kinematical trajectories. Therefore, in this paper, we focused on rhythm control and investigated adaptability at the point of walking rhythm.

Fig. 14 Transition of walking pattern from *straight* to *curved*, carried out by numerical simulations. (**1**) and (**2**) show roll and pitch motions, respectively. **A** and **B** display time-series data of angular velocity at low ($\hat{\beta} = 0.7$) and moderate speeds ($\hat{\beta} = 0.5$), respectively. **C** and **D** show transition of limit cycles of walking patterns at low ($\hat{\beta} = 0.7$) and moderate speeds ($\hat{\beta} = 0.5$), respectively. The point described by $\phi_T = \pi/2$ indicates the state at the moment robot changes walking pattern
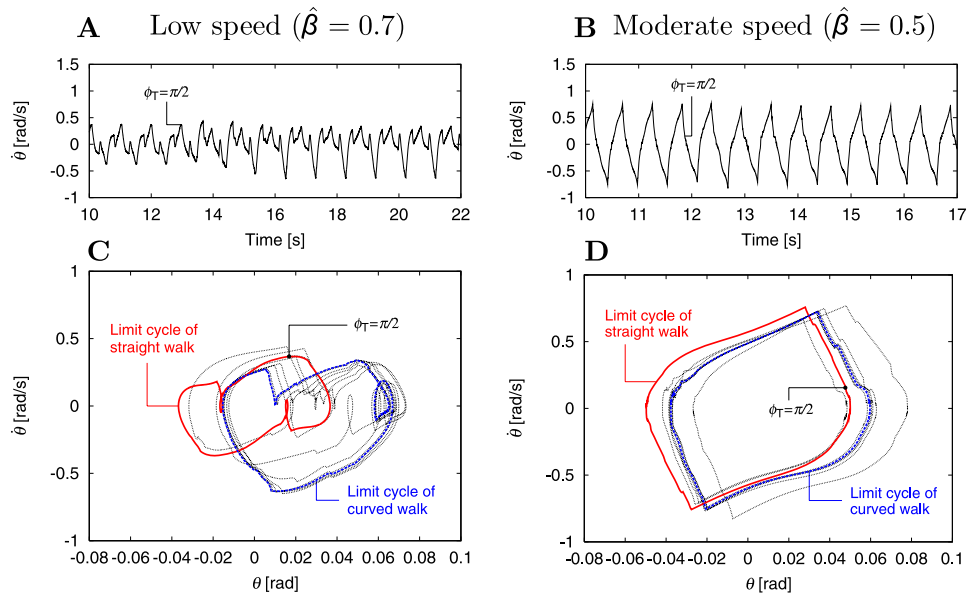
(1) roll motion
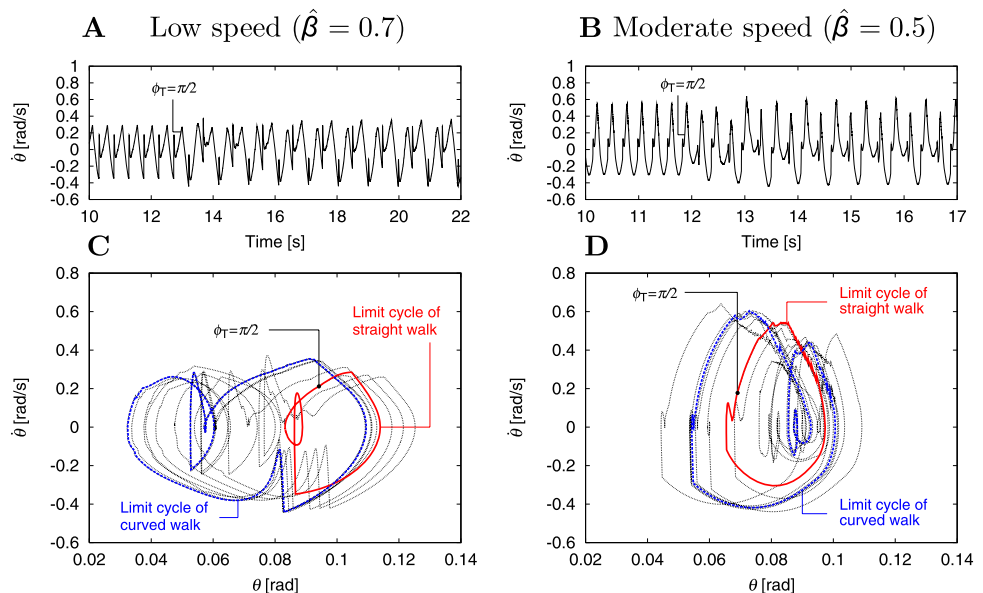
(2) pitch motion

To develop a locomotion control system, we referred to CPG characteristics that generate animal walking by activating their limbs by rhythmic motor patterns and modulating neural activity based on sensory feedbacks. Specifically, we generated robot motions by rhythmic signals from internal oscillators and modulated signal generation based on touch sensor signals. This study demonstrated that a robot achieves adaptive walking by modulation of walking rhythm through interactions between its mechanical system, oscillators, and environment. Furthermore, in curved walking and turning, the robot establishes walking by modulating walking rhythm as well as the walking phase and timing through interactions. This means that in such walking as kinemat-
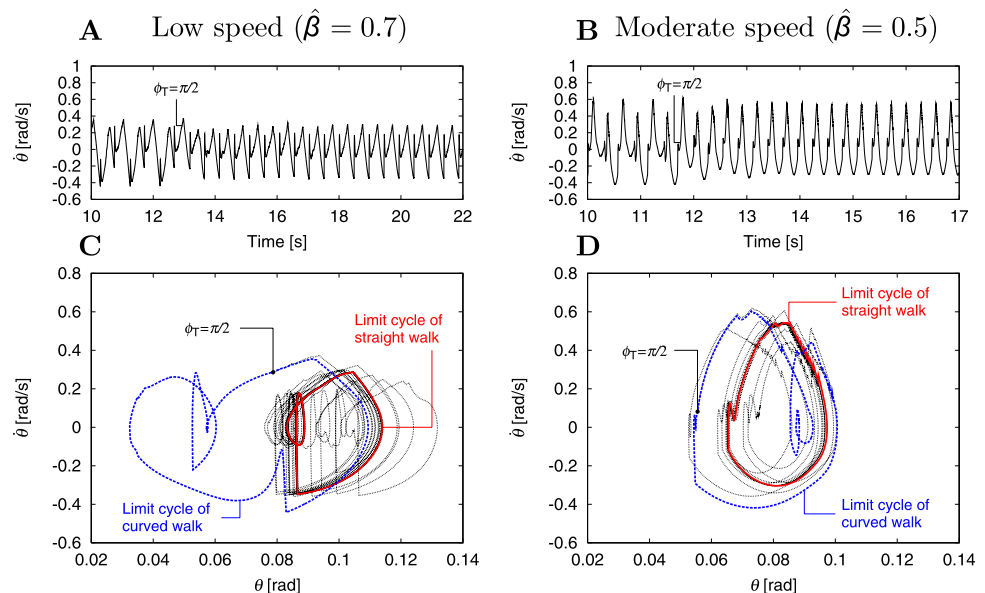
ically symmetric as straight walking, this control system deals with such disturbances as environmental changes by chiefly modulating walking rhythm; in such walking that has kinematical and dynamical asymmetry as turning, this control system deals with disturbances by additionally modulating the walking phase. These results indicate that the control system achieves adaptive walking by appropriately changing its response reflecting the situation due to internal oscillators. As a result, the walking rhythm and phase change.

Many studies on human curved walking and turning have been carried out (Courtine and Schieppati 2003a, 2003b, Grasso et al. 1998; Hollands et al. 2001; Imai et al. 2001;

Fig. 15 Transition of walking pattern from *curved* to *straight*, carried out by numerical simulations. (**1**) and (**2**) show roll and pitch motions, respectively. **A** and **B** display time-series data of the angular velocity at low ($\hat{\beta} = 0.7$) and moderate speeds ($\hat{\beta} = 0.5$), respectively. **C** and **D** show transition of limit cycles of walking patterns at low ($\hat{\beta} = 0.7$) and moderate speeds ($\hat{\beta} = 0.5$), respectively. The point described by $\phi_T = \pi/2$ indicates the state at the moment robot changes walking pattern
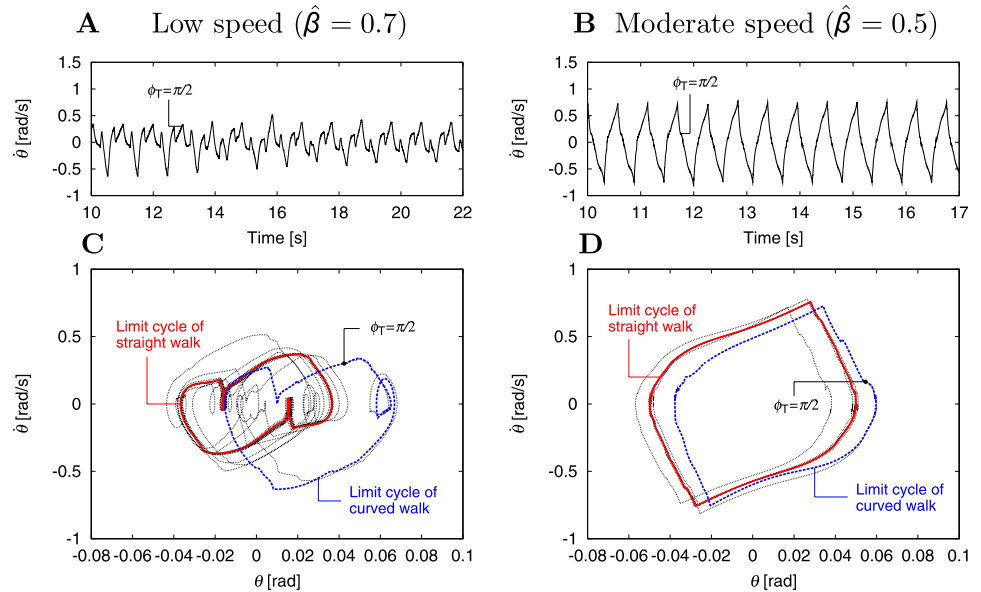
Patla et al. 1999; Thigpen et al. 2000; Vallis et al. 2001). One shared feature is spacial asymmetry, which is the kinematical difference between the right and left limbs. Other characteristics include temporal asymmetry that appears in the resultant duty factors and phase lag between leg motions. As described above, these similar properties are found in the obtained results from numerical simulations and hardware experiments of a biped robot. Admittedly, humans and simple biped robots greatly differ. Humans generate their walking motion by cooperatively manipulating their complicated and redundant musculoskeletal systems. On the other hand, robots have a much smaller number of DOF and com-

pletely different actuators. Furthermore, they have different kinematics during walking and use a much smaller amount of sensory information. However, we employed a simple controller that generates robot joint motions by internal oscillators. In the robot motions, the arms simply oscillate in the pitch plane, the foot trajectory consists of simple closed curve and straight line, and the trunk simply oscillates in the roll plane. This control system only changes the foot trajectory from swing to stance phases and resets the oscillator phases based on touch sensor signals, which don't attempt to achieve similar results as humans. Adaptive behavior in duty factors and phase lag between leg motions appears as a re-

Fig. 16 Basin of attraction of limit cycle in transition of walking pattern from *straight* to *curved*, obtained by numerical simulations. (**1**) and (**2**) show results for roll and pitch motions, respectively
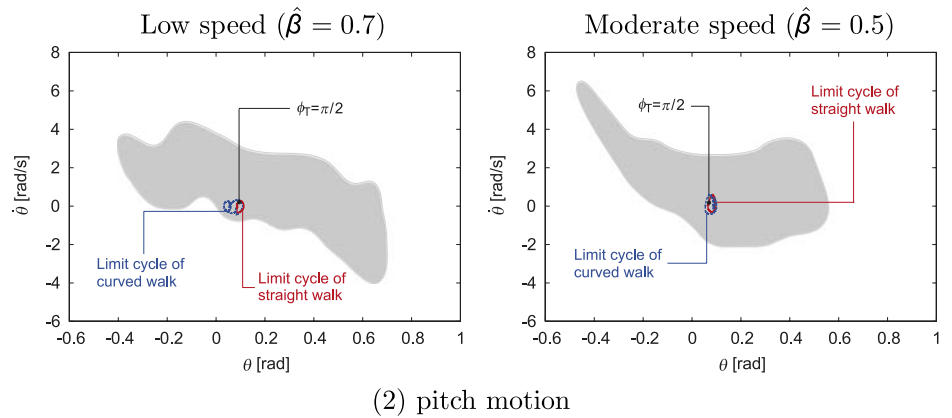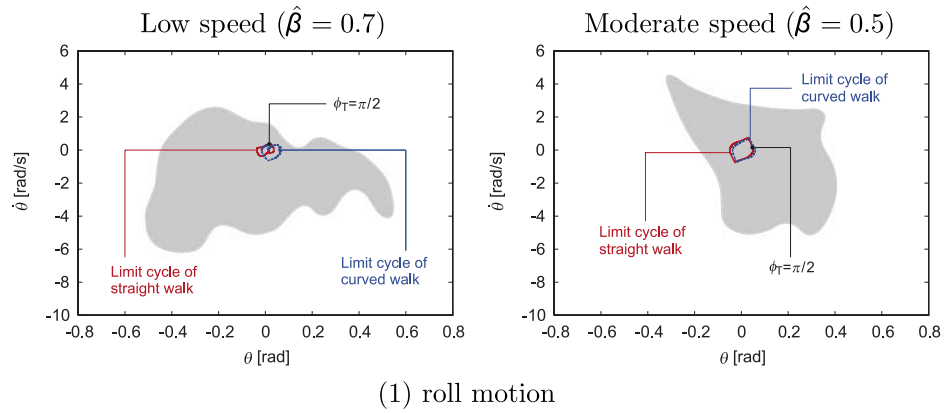

(1) roll motion

(2) pitch motion

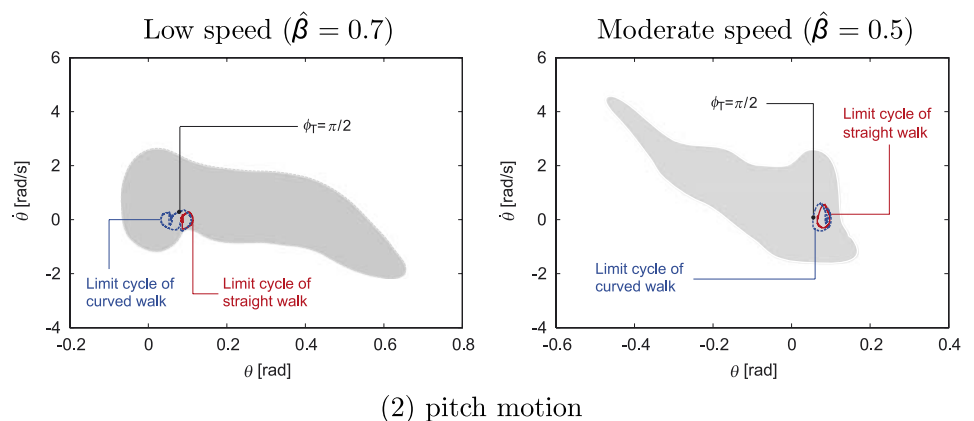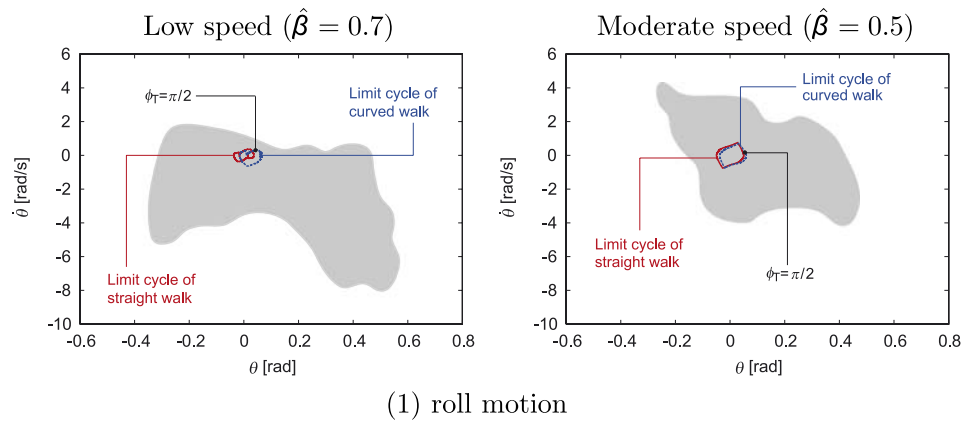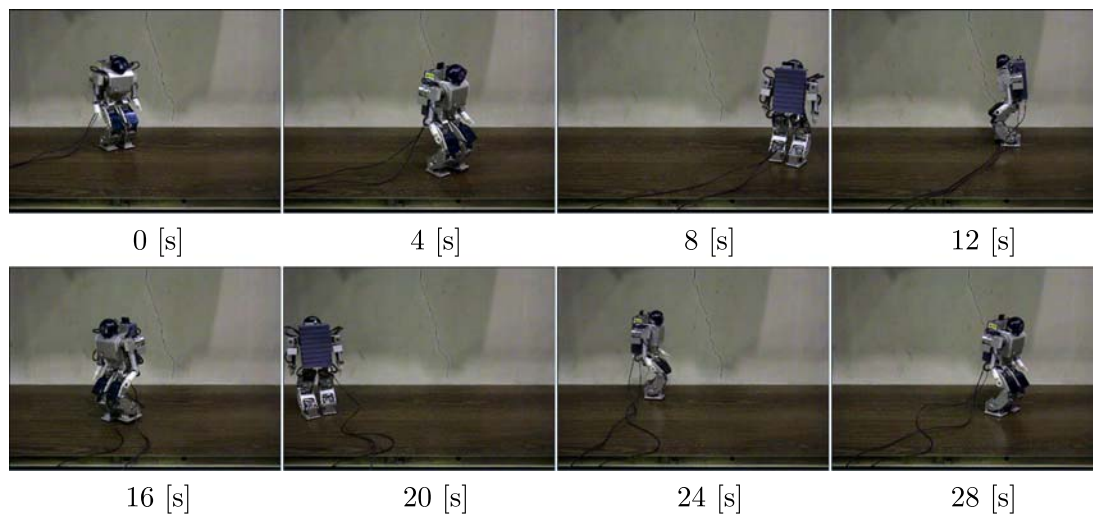**Fig. 17** Basin of attraction of limit cycle in transition of walking pattern from *curved* to *straight*, obtained by numerical simulations. (**1**) and (**2**) show results for roll and pitch motions, respectively

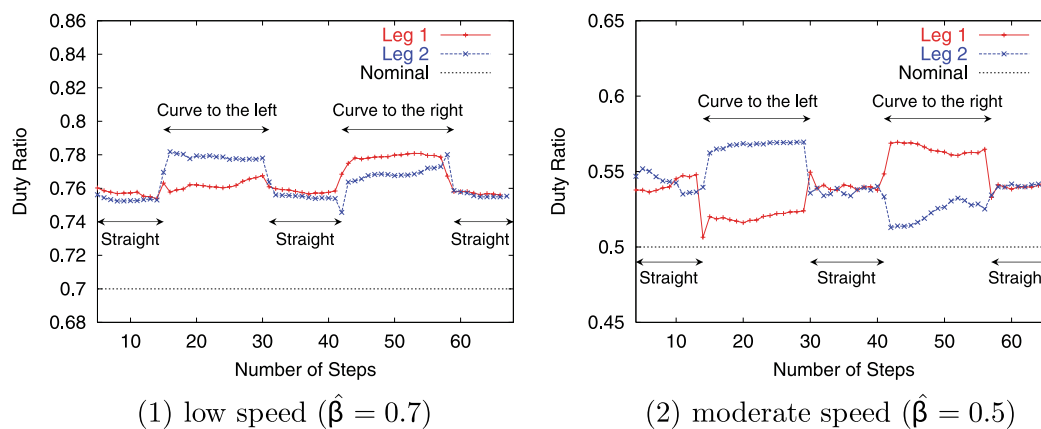

(1) roll motion

(2) pitch motion

A

B

Fig. 18 Transition of walking patterns in hardware experiments. First robot walks straight and then begins to circle to the left. Next, the its motion returns to straight walking and changes to curved walking to the right. Finally, it walks straight again. **A** shows snapshots during transition at moderate speed ($\hat{\beta} = 0.5$). By regulating the number of steps for each walking pattern, robot walks in a figure eight. **B(1)** and (**2**) show resultant duty factors of left leg β^1 and right leg β^2 with respect to each step at low ($\hat{\beta} = 0.7$) and moderate speeds ($\hat{\beta} = 0.5$), respectively

sult of the adequate modulations of the internal oscillators. Therefore, if these factors reflect the essential ingredients that generate walking, such similarity may demonstrate an important mechanism for establishing adaptive behavior for biped robots.

6.2 Advanced turning behavior

For conventional approaches including model-based, the difficulty of achieving adaptability to various environments is often pointed out. Adaptive behavior requires adequate modulations of motions and responses depending on the situation. That is, in these approaches, robots are too rigid to appropriately react to various situations. In this study, we designed a control system composed of nonlinear oscillators

that adequately responds based on environmental situations and established a soft robot that achieves adaptive behavior.

This study is basic research that investigates the mechanism to establish adaptive behavior for biped robots. Therefore, we employed a simple control system and strategy to avoid restricting the possibility of applications and to determine the essentials. This control system needed neither accurate modeling of the robot and the environment nor complicated computations. For example, to change its walking direction, instead of calculating the foot landing positions, the robot just changes the stepping direction of the swing leg. It uses neither a vision system nor postural information relative to the ground. It just relies on the timing of the touch sensor signals.

This study demonstrated that a simple structure can explain the mechanism for adaptive behavior; it didn't pursue

the performance of walking motions. Therefore, the control system has limitations. There must be kinematically and dynamically more advanced turning strategies, control methods, and motion generation, as achieved in various studies (Hirai et al. 1998; Ishida et al. 2003; Kagami et al. 2002; Kajita et al. 2002; Löffler et al. 2003; Seara and Schmidt 2004). In the future, improving the control system by integrating robot kinematics and dynamics and more various sensory information is important, where clarified essential properties inherent in walking dynamics will be helpful to generate more advanced behavior.

7 Conclusion

In this study, we analyzed the turning behavior of a biped robot and considered turning that consisted of straight and curved walking and the transition between them. We referred to CPG properties and investigated adaptability to generate such turning motion at the point of rhythm control. In particular, we proposed a locomotion control system that generates robot motions by rhythmic signals from internal oscillators and modulates signal generation based on touch sensor signals. First, we verified that the robot attains the limit cycles of straight and curved walking by numerical simulations and hardware experiments. Second, we examined the transition of these walking patterns based on the basin of attraction of the limit cycles in numerical simulations. Finally, we verified that the robot actually achieves transition and turning by using hardware experiments. These analyses revealed that the robot establishes stable walking and turning by modulation of walking rhythm and phase through the interactions between the dynamics of its mechanical system, oscillators, and environment.

References

Akimoto, K., Watanabe, S., & Yano, M. (1999). An insect robot controlled by emergence of gait patterns. *Artificial Life and Robotics*, *3*, 102–105.

Altendorfer, R., Moore, N., Komsuoglu, H., Buehler, M., Brown, H. B., Jr., McMordie, D., Saranli, U., Full, R., & Koditschek, D. E. (2001). RHex: A biologically inspired hexapod runner. *Autonomous Robots*, *11*(3), 207–213.

Aoi, S., & Tsuchiya, K. (2005). Locomotion control of a biped robot using nonlinear oscillators. *Autonomous Robots*, *19*(3), 219–232.

Aoi, S., & Tsuchiya, K. (2006a). Bifurcation and chaos of a simple walking model driven by a rhythmic signal. *International Journal of Non-Linear Mechanics*, *41*(3), 438–446.

Aoi, S., & Tsuchiya, K. (2006b). Stability analysis of a simple walking model driven by an oscillator with a phase reset using sensory feedback. *IEEE Transactions on Robotics*, *22*(2), 391–397.

Aoi, S., & Tsuchiya, K. (2007). Self-stability of a simple walking model driven by a rhythmic signal. *Nonlinear Dynamics*, *48*(1–2), 1–16.

Aoi, S., Sasaki, H., & Tsuchiya, K. (2007). A multilegged modular robot that meanders: Investigation of turning maneuvers using its inherent dynamic characteristics, *SIAM Journal on Applied Dynamical Systems*.

Brockett, R. W. (2003). Pattern generation and the control of nonlinear systems. *IEEE Transactions on Automatic Control*, *48*(10), 1699–1711.

Cham, J. G., Karpick, J. K., & Cutkosky, M. R. (2004). Stride period adaptation of a biomimetic running hexapod. *International Journal of Robotics Research*, *23*(2), 141–153.

Courtine, G., & Schieppati, M. (2003a). Human walking along a curved path. I. Body trajectory, segment orientation and the effect of vision. *European Journal of Neuroscience*, *18*(1), 177–190.

Courtine, G., & Schieppati, M. (2003b). Human walking along a curved path. II. Gait features and EMG patterns. *European Journal of Neurosience*, *18*(1), 191–205.

Crespi, A., Badertscher, A., Guignard, A., & Ijspeert, A. J. (2005). AmphiBot I: An amphibious snake-like robot. *Robotics and Autonomous Systems*, *50*(4), 163–175.

Fukuoka, Y., Kimura, H., & Cohen, A. H. (2003). Adaptive dynamic walking of a quadruped robot on irregular terrain based on biological concepts. *International Journal of Robotics Research*, *22*(3–4), 187–202.

Grasso, R., Assaiante, C., Prévost, P., & Berthoz, A. (1998). Development of anticipatory orienting strategies during locomotor tasks in children. *Neuroscience Biobehavioral Reviews*, *22*, 533–539.

Grillner, S. (1981). Control of locomotion in bipeds, tetrapods and fish. In *Handbook of Physiology* (pp. 1179–1236). Bethesda: American Physiological Society.

Grillner, S. (1985). Neurobiological bases of rhythmic motor acts in vertebrates. *Science*, *228*, 143–149.

Hase, K., & Stein, R. B. (1999). Turning strategies during human walking. *Journal of Neurophysiology*, *81*(6), 2914–2922.

Hollands, M., Sorensen, K., & Patla, A. (2001). Effects of head immobilization on the coordination and control of head and body reorientation and translation during steering. *Experimental Brain Research*, *140*(2), 223–233.

Hirai, K., Hirose, M., Haikawa, Y., & Takenaka, T. (1998). The development of the Honda humanoid robot. In *Proceedings of the IEEE international conference on robotics and automation* (pp. 1321–1326).

Ijspeert, A. J., Crespi, A., & Cabelguen, J. M. (2005). Simulation and robotics studies of salamander locomotion. Applying neurobiological principles to the control of locomotion in robots. *Neuroinformatics*, *3*(3), 171–196.

Ijspeert, A. J., Crespi, A., Ryczko, D., & Cabelguen, J. M. (2007). From swimming to walking with a salamander robot driven by a spinal cord model. *Science*, *315*(5817), 1416–1420.

Imai, T., Moore, S. T., Raphan, T., & Cohen, B. (2001). Interaction of the body, head, and eyes during walking and turning. *Experimental Brain Research*, *136*, 1–18.

Inagaki, S., Yuasa, H., & Arai, T. (2003). CPG model for autonomous decentralized multi-legged robot system—generation and transition of oscillation patterns and dynamics of oscillators. *Robotics and Autonomous Systems*, *44*(3–4), 171–179.

Inoue, K., Ma, S., & Jin, C. (2004). Neural oscillator network-based controller for meandering locomotion of snake-like robots. In *Pro-

ceedings of the IEEE international conference on robotics and automation (pp. 5064–5069).

Ishida, T., Kuroki, Y., & Yamaguchi, J. (2003). Mechanical system of a small biped entertainment robot. In *Proceedings of the IEEE/RSJ international conference on intelligent robots and systems* (pp. 1129–1134).

Kagami, S., Nishiwaki, K., Kuffner, J., Kuniyoshi, Y., Inaba, M., & Inoue, H. (2002). Online 3D vision, motion planning and bipedal locomotion control coupling system of humanoid robot: H7. In *Proceedings of the IEEE/RSJ international conference on intelligent robots and systems* (pp. 2557–2562).

Kajita, S., Kanehiro, F., Kaneko, K., Fujiwara, K., Yokoi, K., & Hirukawa, H. (2002). A realtime pattern generator for biped walking. In *Proceedings IEEE international conference on robotics and automation* (pp. 31–37).

Kimura, H., Akiyama, S., & Sakurama, K. (1999). Realization of dynamic walking and running of the quadruped using neural oscillator. *Autonomous Robots*, *7*(3), 247–258.

Lewis, M. A., & Bekey, G. A. (2002). Gait adaptation in a quadruped robot. *Autonomous Robots*, *12*, 301–312.

Lewis, M. A., Etienne-Cummings, R., Hartmann, M. J., Xu, Z. R., & Cohen, A. H. (2003). An in silico central pattern generator: Silicon oscillator, coupling, entrainment, and physical computation. *Biological Cybernetics*, *88*, 137–151.

Löffler, K., Gienger, M., & Pfeiffer, F. (2003). Sensors and control concept of walking "Johnnie. *International Journal of Robotics Research*, *22*(3–4), 229–239.

Mori, S. (1987). Integration of posture and locomotion in acute decerebrate cats and in awake, free moving cats. *Progress in Neurobiology*, *28*, 161–196.

Laszlo, J. F. (1996). Limit cycle control and its application to the animation of balancing and walking. In *Proceedings of the SIGGRAPH'96* (pp. 155–162).

Nakanishi, J., Morimoto, J., Endo, G., Cheng, G., Schaal, S., & Kawato, M. (2004). Learning from demonstration and adaptation of biped locomotion. *Robotics and Autonomous Systems*, *47*, 79–91.

Nakanishi, M., Nomura, T., & Sato, S. (2006). Stumbling with optimal phase reset during gait can prevent a humanoid from falling. *Biolgical Cybernetics*, *95*(5), 503–515.

Nilsson, J., & Thorstensson, A. (1989). Ground reaction forces at different speeds of human walking and running. *Acta Physiologica Scandinavica*, *136*(2), 217–227.

Ogihara, N., & Yamazaki, N. (2001). Generation of human bipedal locomotion by a bio-mimetic neuro-musculo-skeletal model. *Biological Cybernetics*, *84*, 1–11.

Orlovsky, G. N., Deliagina, T., & Grillner, S. (1999). *Neuronal control of locomotion: From mollusc to man*. Oxford: Oxford University Press.

Patla, A. E., Adkin, A., & Ballard, T. (1999). Online steering: coordination and control of body center of mass, head and body reorientation. *Experimental Brain Research*, *129*(4), 629–634.

Poulakakis, I., Smith, J. A., & Buehler, M. (2005). Modeling and experiments of untethered quadrupedal running with a bounding gait: The Scout II Robot. *International Journal of Robotics Research*, *24*(4), 239–256.

Quinn, R. D., Nelson, G. M., Bachmann, R. J., Kingsley, D. A., Offi, J. T., Allen, T. J., & Ritzmann, R. E. (2003). Parallel complementary strategies for implementing biological principles into mobile robots. *International Journal of Robotics Research*, *22*(3), 169–186.

Righetti, L., & Ijspeert, A. J. (2006). Programmable central pattern generators: an application to biped locomotion control. In *Proceedings of the IEEE international conference on robotics and automation* (pp. 1585–1590).

Rossignol, S. (1996). *Neural control of stereotypic limb movements*. Oxford: Oxford University Press.

Saranli, U., Buehler, M., & Koditschek, D. E. (2001). RHex: A simple and highly mobile hexapod robot. *International Journal of Robotics Research*, *20*(7), 616–631.

Seara, J. F., & Schmidt, G. (2004). Intelligent gaze control for vision-guided humanoid walking: methodological aspects. *Robotics and Autonomous Systems*, *48*(4), 231–248.

Taga, G., Yamaguchi, Y., & Shimizu, H. (1991). Self-organized control of bipedal locomotion by neural oscillators in unpredictable environment. *Biological Cybernetics*, *65*, 147–159.

Taga, G. (1995a). A model of the neuro-musculo-skeletal system for human locomotion, I: Emergence of basic gait. *Biological Cybernetics*, *73*, 97–111.

Taga, G. (1995b). A model of the neuro–musculo–skeletal system for human locomotion, II: Real-time adaptability under various constraints. *Biological Cybernetics*, *73*, 113–121.

Takakusaki, K., Habaguchi, T., Ohtinata-Sugimoto, J., Saitoh, K., & Sakamoto, T. (2003). Basal ganglia efferents to the brainstem centers controlling postural muscle tone and locomotion; A new concept for understanding motor disorders in basal ganglia dysfunction. *Neuroscience*, *119*, 293–308.

Takakusaki, K., Saitoh, K., Harada, H., & Kashiwayanagi, M. (2004). Role of basal ganglia-brainstem pathways in the control of motor behaviors. *Neuroscience Research*, *50*, 137–151.

Takuma, T., & Hosoda, K. (2006). Controlling the walking period of a pneumatic muscle walker. *International Journal of Robotics Research*, *25*(9), 861–866.

Thigpen, M. T., Light, K. E., Creel, G. L., & Flynn, S. M. (2000). Turning difficulty characteristics of adults aged 65 years or older. *Physical Therapy*, *80*(12), 1174–1187.

Tomita, N., & Yano, M. (2004). A model of bipedal walking controlled by the basal ganglia-brainstem systems. In *Proceedings of the 9th international symposium on artificial life and robotics* (pp. 359–362).

Tsujita, K., Tsuchiya, K., & Onat, A. (2001). Adaptive gait pattern control of a quadruped locomotion robot. In *Proceedings of the IEEE/RSJ international conference on intelligent robots and systems* (pp. 2318–2325).

Vallis, L. A., Patla, A. E., & Adkin, A. L. (2001). Control of steering in the presence of unexpected head yaw movements Influence on sequencing of subtasks. *Experimental Brain Research*, *138*(1), 128–134.

Vukobratović, M., Borovac, B., Surla, D., & Stokić, D. (1990). *Biped locomotion-dynamics, stability, control and application*. Berlin: Springer.

Wisse, M., Schwab, A. L., van der Linde, R. Q., & van der Helm, F. C. T. (2005). How to keep from falling forward: elementary swing leg action for passive dynamic walkers. *IEEE Transactions on Robotics*, *21*(3), 393–401.

Yamasaki, T., Nomura, T., & Sato, S. (2003). Possible functional roles of phase resetting during walking. *Biological Cybernetics*, *88*, 468–496.

Shinya Aoi received the B.E., M.E., and Ph.D. degrees from the Department of Aeronautics and Astronautics, Kyoto University, Kyoto, Japan in 2001, 2003, and 2006, respectively. From 2003 to 2006, he was a research fellow of the Japan Society for the Promotion of Science (JSPS). Since 2006, he has been a COE research associate at Kyoto University, Kyoto, Japan. His research interests include dynamics and control of robotic systems, especially legged robots. He is a member of IEEE, SICE, and RSJ.

Kazuo Tsuchiya received the B.S., M.S., and Ph.D. degrees in engineering from Kyoto University, Kyoto, Japan in 1966, 1968, and 1975, respectively. From 1968 to 1990, he was a research member of Central Research Laboratory in Mitsubishi Electric Corporation, Amagasaki, Japan. From 1990 to 1995, he was a professor at the Department of Computer Controlled Machinery, Osaka University, Osaka, Japan. Since 1995, he has been a professor at the Department of Aeronautics and Astronautics, Kyoto University. His fields of research include dynamic analysis, guidance, and control of space vehicles, and nonlinear system theory for distributed autonomous systems. He is currently the principal investigator of "Research and Education on Complex Functional Mechanical Systems" under the 21st Century Center of Excellence Program (COE program of the Ministry of Education, Culture, Sports, Science and Technology, Japan).